

Demand Response for Flat Nonlinear MIMO Processes using Dynamic Ramping Constraints

Florian Joseph Baader^{a,b,c,*}, Philipp Althaus^{a,c}, André Bardow^{a,b}, Manuel Dahmen^a

^a Forschungszentrum Jülich GmbH, Institute of Energy and Climate Research, Energy Systems Engineering (IEK-10), Jülich 52425, Germany

^b ETH Zürich, Energy & Process Systems Engineering, Zürich 8092, Switzerland

^c RWTH Aachen University Aachen 52062, Germany

Abstract: Volatile electricity prices make demand response (DR) attractive for processes that can modulate their production rate. However, if nonlinear dynamic processes must be scheduled simultaneously with their local multi-energy system, the resulting scheduling optimization problems often cannot be solved in real time. For single-input single-output processes, the problem can be simplified without sacrificing feasibility by dynamic ramping constraints that define a derivative of the production rate as the ramping degree of freedom. In this work, we extend dynamic ramping constraints to flat multi-input multi-output processes by a coordinate transformation that gives the true nonlinear ramping limits. Approximating these ramping limits by piecewise affine functions gives a mixed-integer linear formulation that guarantees feasible operation. As a case study, dynamic ramping constraints are derived for a heated reactor-separator process that is subsequently scheduled simultaneously with its multi-energy system. The dynamic ramping formulation bridges the gap between rigorous process models and simplified process representations for real-time scheduling.

Keywords:

Demand response, Mixed-integer dynamic optimization, Flatness, Simultaneous scheduling

arXiv:2205.14598v3 [math.OC] 24 Oct 2022

*F. J. Baader, ETH Zürich, Energy & Process Systems Engineering, Zürich 8092, Switzerland
E-mail: fbaader@ethz.ch

1 Introduction

Reducing greenhouse gas emissions requires increased renewable electricity production that, however, gives a fluctuating supply. This fluctuating supply can be compensated by consumers that react to time-varying electricity prices by shifting their demand in time in a so-called demand response (DR) (Zhang and Grossmann, 2016). DR can be attractive for energy-intensive production processes with the flexibility to modulate their production rate. To exploit the DR potential, a scheduling optimization is needed, which typically determines operational set-points for a time horizon in the order of one day (Baldea and Harjunkski, 2014). However, such a scheduling optimization is computationally challenging for nonlinear processes that exhibit scheduling-relevant dynamics. The scheduling optimization becomes even more difficult if processes do not only consume electricity but also heating or cooling as these processes need to be scheduled simultaneously with the local multi-energy supply system (often also referred to as utility system) (Leenders et al., 2019). Local multi-energy supply systems bring integer on/off decisions into the scheduling optimization, especially as they often consist of multiple redundant units (Voll et al., 2013). Thus, the simultaneous scheduling optimization problem usually is a nonlinear mixed-integer dynamic optimization (MIDO) problem (Baader et al., 2022c).

Traditionally, such challenging scheduling MIDO problems are simplified by introducing static ramping constraints that define the rate of change of the production rate ρ as degree of freedom ν and limit ν with constant ramping limits ν^{\min} , ν^{\max} , see e.g., Carrion and Arroyo (2006); Mitra et al. (2012); Adamson et al. (2017); Zhou et al. (2017); Hoffmann et al. (2021):

$$\dot{\rho} = \nu \text{ with } \nu^{\min} \leq \nu \leq \nu^{\max} \quad (1)$$

If additionally, the nonlinear energy demand of the production process is approximated as a piecewise-affine (PWA) function, the complete problem can be reformulated as a mixed-integer linear program (MILP) (Schäfer et al., 2020).

Traditional ramping constraints, however, have two shortcomings: They are restricted to (i) first-order dynamics and (ii) constant ramping limits. To tackle both shortcomings, we proposed high-order dynamic ramping constraints in our previous publication (Baader et al., 2022a). These high-order dynamic ramping constraints limit the δ -th derivative of the production rate ρ and use limits ν^{\min} , ν^{\max} which are functions of the production rate and its time derivatives:

$$\rho^{(\delta)} = \nu \text{ with } \nu^{\min}(\rho, \dot{\rho}, \dots, \rho^{(\delta-1)}) \leq \nu \leq \nu^{\max}(\rho, \dot{\rho}, \dots, \rho^{(\delta-1)}) \quad (2)$$

Dynamic ramping constraints allow to represent energy-intensive processes better than static ones due to their ability to account for high-order dynamics and non-constant ramping limits that depend on the process state. In Baader et al. (2022a), we demonstrated that dynamic ramping constraints can achieve solutions of the scheduling optimization problem that are close to the solutions of the original nonlinear MIDO problem while allowing to formulate MILPs that can be solved sufficiently fast for real-time scheduling. Moreover, we presented a method to derive dynamic ramping constraints rigorously for the special case of single-input single-output (SISO) processes that are exact input-state linearizable. However, this case is quite restrictive, and the question remained how to derive dynamic ramping constraints for more general processes. In particular, it was open how to apply the dynamic ramping method to multi-input multi-output (MIMO) processes that have a variable production rate ρ while, at the same time, other output variables \mathbf{y} such as temperatures and concentrations need to be controlled using a set of control inputs \mathbf{u} (Figure 1).

The present publication extends the dynamic ramping approach to MIMO processes and presents a method to derive dynamic ramping constraints rigorously for differentially flat MIMO processes. In simple words, a MIMO process with m inputs is differentially flat if an output vector $\boldsymbol{\xi}$ of the same size m exists such that all process states and inputs can be given as a function of the output $\boldsymbol{\xi}$ and its β time derivatives $\dot{\boldsymbol{\xi}}$, ..., $\boldsymbol{\xi}^{(\beta)}$ (Fliess et al., 1995; Rothfuß, 1997; Rothfuß et al., 1996). We make use of the fact that a flat nonlinear model can be transformed to a linear model (Fliess et al., 1995). However, constraints that are linear for the original model, e.g., bounds on inputs, are nonlinear for the transformed model. In other words, a nonlinear model with linear constraints is transformed into a linear model with nonlinear constraints. Approximating the nonlinear bounds to the safe side with piecewise-affine functions allows us

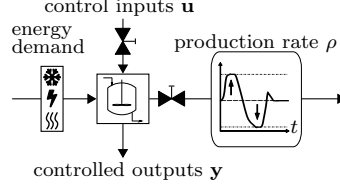


Fig. 1. A MIMO process that can vary its production rate ρ and thus its energy demand while additional control inputs \mathbf{u} are available to control further process outputs variables \mathbf{y} .

to formulate a MILP, whose solution is guaranteed to be feasible also for the non-approximated version. Note that for SISO processes, flatness is equivalent to exact input-state linearizability (Adamy, 2014), which was the main assumption in our previous work (Baader et al., 2022a). For MIMO processes, exact input-state linearizability with static state transformation is a special case of flatness (Adamy, 2014).

The remaining paper is structured as follows: In Section 2, the considered demand response optimization problem and the dynamic ramping constraints are introduced. In Section 3, a method is presented to derive dynamic ramping constraints for flat MIMO processes. In Section 4, a case study is presented. Section 5 provides further discussion and Section 6 concludes the work.

2 Dynamic mixed-integer linear scheduling with ramping constraints

This section briefly introduces the simultaneous scheduling optimization problem (P) of flexible processes represented by dynamic ramping constraints and multi-energy supply systems. This problem is a mixed-integer dynamic optimization (MIDO) problem with linear and piecewise affine (PWA) functions. We discretize time through collocation on finite elements (Biegler, 2010) to convert the MIDO problem (P) to a MILP. The size of the final MILP problem is proportional to the number of discretization points. Note that all decision variables $\chi = (\nu, (\mathbf{Q}_{\text{dem}}^{\text{process}})^T, \rho, S, \Phi_{\text{energy}}, (\mathbf{Q}^{\text{in}})^T, (\mathbf{Q}^{\text{out}})^T, (\Delta \mathbf{P})^T, \mathbf{z}_{\text{on}}^T)^T$, which are introduced in the following, are functions of time t . Still, we do not state time dependency explicitly to ease readability. The problem (P) without time discretization reads:

$$\begin{aligned}
 & \min_{\chi \in [\chi^l, \chi^u]} \Phi_{\text{energy}}(t_f) & (\text{Pa}) \\
 \text{s.t.} \quad & \text{Dynamic ramping constraints} & (\text{Pb}) \\
 & \text{Process energy demand model} & (\text{Pc}) \\
 & \text{Product storage: } \dot{S} = \rho - \rho^{\text{nom}} \quad \forall t \in \mathbb{T} & (\text{Pd}) \\
 & \text{Energy costs: } \dot{\Phi}_{\text{energy}} = \sum_{e \in \mathbb{E}} p_e \left(\sum_{i \in \mathbb{C}_e^{\text{cons}}} Q_i^{\text{in}} + \Delta P_e \right) \quad \forall t \in \mathbb{T} & (\text{Pe}) \\
 & \text{Energy conversion: } Q_i^{\text{out}} = h_{Q_i^{\text{out}}}^{\text{PWA}}(Q_i^{\text{in}}) \quad \forall i \in \mathbb{C}, \forall t \in \mathbb{T} & (\text{Pf}) \\
 & \text{Minimum part-load: } z_i^{\text{on}} Q_i^{\text{min}} \leq Q_i^{\text{out}} \leq z_i^{\text{on}} Q_i^{\text{max}}, \quad \forall i \in \mathbb{C}, \forall t \in \mathbb{T} & (\text{Pg}) \\
 & \text{Balances: } Q_{\text{dem},e}^{\text{process}} + Q_{\text{dem},e}^{\text{inflexible}} = \sum_{i \in \mathbb{C}_e^{\text{sup}}} Q_i^{\text{out}} + \Delta P_e, \quad \forall e \in \mathbb{E}, \forall t \in \mathbb{T} & (\text{Ph})
 \end{aligned}$$

The objective is to minimize the cumulative energy costs Φ_{energy} at final time t_f . The lower and upper bounds of the decision variables are χ^l and χ^u . In the following paragraph, we discuss the dynamic ramping constraints (Pb) and the process energy demand model (Pc) in detail. The remaining constraints (Pd) to (Ph) are standard constraints (Schäfer et al., 2020; Sass et al., 2020) and discussed in more detail in our previous publication (Baader et al., 2022a). Thus, we only briefly introduce the symbols here. All decision variables are functions of time $t \in \mathbb{T}$ although not stated explicitly to ease readability. The

product storage with level S is filled by the production rate ρ and emptied with the nominal production ρ^{nom} (Pd). The rate of change of the energy costs Φ_{energy} is the price of an energy form e , p_e times the input power Q_i^{in} of energy conversion units consuming e , \mathbb{C}_e , and the power exchanged with the grid ΔP_e . The set \mathbb{E} in (Pe) covers all considered energy forms. For the energy conversion of a components i in the set of components \mathbb{C} , the output power Q_i^{out} is given as piecewise affine function $h_{Q_i^{\text{out}}}^{\text{PWA}}$ of the input power Q_i^{in} (Pf). Additionally, minimum part-load is modeled with a binary variable z_i^{on} to ensure the output power Q_i^{out} is either zero or between minimum part-load Q_i^{min} and maximum power Q_i^{max} (Pg). Finally, the energy balances state that the demands of the flexible process $Q_{\text{dem},e}^{\text{process}}$ and the demands of other inflexible processes $Q_{\text{dem},e}^{\text{inflexible}}$ have to be satisfied by the output Q_i^{out} of energy conversion units supplying energy e , collected in set $\mathbb{C}_e^{\text{sup}}$, and power from the grid ΔP_e (Ph).

In our previous publication (Baader et al., 2022a), we only derived dynamic ramping constraints (Pb) for processes with a single input. We, therefore, only had to constrain a single time derivative of the production rate ρ with order δ , which we defined as the ramping degree of freedom $\nu = \rho^{(\delta)}$. In the present contribution, we consider multiple inputs \mathbf{u} and can potentially have constraints on all considered derivatives of the production rate $\rho^{(\gamma)}$ with $\gamma = 1, \dots, \delta$ and the integer δ being the order of the highest time derivative that is constrained by input bounds. For instance, the bounds of input u_1 could directly limit the first derivative of the production rate, $\dot{\rho}$, whereas the bounds on input u_2 could limit the second derivative of the production rate, $\rho^{(2)}$, directly and only influence the first derivative, $\dot{\rho}$, through the integration. The generalized dynamic ramping constraints (DRCs) developed in this publication therefore read:

$$\rho^{(\delta)} = \nu \quad (\text{DRCa})$$

$$\dot{\rho}^{\text{min}}(\rho) \leq \dot{\rho} \leq \dot{\rho}^{\text{max}}(\rho) \quad (\text{DRCb})$$

$$\vdots$$

$$\left(\rho^{(\gamma)}\right)^{\text{min}}\left(\rho, \dot{\rho}, \dots, \rho^{(\gamma-1)}\right) \leq \rho^{(\gamma)} \leq \left(\rho^{(\gamma)}\right)^{\text{max}}\left(\rho, \dot{\rho}, \dots, \rho^{(\gamma-1)}\right) \quad (\text{DRCc})$$

$$\vdots$$

$$\nu^{\text{min}}\left(\rho, \dot{\rho}, \dots, \rho^{(\delta-1)}\right) \leq \nu \leq \nu^{\text{max}}\left(\rho, \dot{\rho}, \dots, \rho^{(\delta-1)}\right) \quad (\text{DRCd})$$

Still, only the highest considered time derivative $\rho^{(\delta)}$ is a degree of freedom and thus defined as the ramping degree of freedom ν .

The limits $(\rho^{(\gamma)})^{\text{min}}$, $(\rho^{(\gamma)})^{\text{max}}$ as well as ν^{min} , ν^{max} are in general nonlinear functions that we derive by coordinate transformation (Section 3). To incorporate the dynamic ramping constraint into an MILP formulation, the true nonlinear limits are approximated by piecewise-affine (PWA) functions for all considered derivatives $\gamma = 1, \dots, \delta$ because PWA functions allow us to formulate a mixed-integer linear scheduling problem. These piecewise-affine functions need to be conservative such that they prohibit constraint violation with respect to the true nonlinear limits to guarantee that the chosen trajectory for ρ satisfies all bounds on inputs and states. Accordingly, the approximations of $(\rho^{(\gamma)})^{\text{min}}$ and ν^{min} must always be greater than or equal to the true nonlinear limits and the approximations of $(\rho^{(\gamma)})^{\text{max}}$ and ν^{max} must always be lower than or equal to the real nonlinear limits. Choosing the quality of the approximations allows us to explicitly balance the achievable flexibility range against the computational burden.

The process energy demand $Q_{\text{dem},e}$ (cf. Equation (Pc)) for an energy form e is modeled as a function of the production rate and its time derivatives:

$$Q_{\text{dem},e}^{\text{process}}\left(\rho, \dot{\rho}, \dots, \rho^{(\delta-1)}, \nu\right) \quad (3)$$

Similar to the DRC, a piecewise-affine function is chosen for $Q_{\text{dem},e}^{\text{process}}$ to achieve an MILP formulation.

The problem formulation (P) with DRCs captures a larger share of the dynamic flexibility range of processes than static ramping constraints can do while still allowing to formulate a mixed-integer linear

program. However, to choose suitable piecewise-affine ramping limits, the true nonlinear limits of the process need to be derived or approximated. In the following section, we show how these limits can be derived rigorously for MIMO processes that are differentially flat.

3 Deriving dynamic ramping constraints

In Section 3.1, necessary assumptions are stated and then our approach is presented in Section 3.2.

3.1 Assumptions

1. The process degrees of freedom are divided into a control input vector \mathbf{u} and the variable production rate ρ . The process model is a system of ordinary differential equations given by:

$$\dot{\mathbf{x}} = \mathbf{f}(\mathbf{x}, \mathbf{u}, \rho) \quad (4)$$

with state vector $\mathbf{x} \in \mathbb{R}^n$, and a nonlinear right-hand side function $\mathbf{f}(\mathbf{x}, \mathbf{u}, \rho)$. We assume that there are no further inputs or disturbances to the process.

2. The control input vector \mathbf{u} , and the production rate ρ are bounded by minimum and maximum values \mathbf{u}^{\min} , \mathbf{u}^{\max} , and ρ^{\min} , ρ^{\max} , respectively. Similarly, the states \mathbf{x} have to be maintained within bounds \mathbf{x}^{\min} , \mathbf{x}^{\max} .
3. The process (4) is flat. That is, the process has one or multiple flat output vectors $\boldsymbol{\xi}$. An output vector $\boldsymbol{\xi}$ is flat if it satisfies three conditions (Fliess et al., 1995; Rothfuß, 1997; Rothfuß et al., 1996):

- (a) The flat output vector can be given as a function $\boldsymbol{\phi}$ of states \mathbf{x} , inputs \mathbf{u} , production rate ρ , and time derivatives of \mathbf{u} and ρ :

$$\boldsymbol{\xi} = \boldsymbol{\phi} \left(\mathbf{x}, \mathbf{u}, \dot{\mathbf{u}}, \dots, \mathbf{u}^{(\alpha)}, \rho, \dot{\rho}, \dots, \rho^{(\kappa)} \right) \quad (5a)$$

with finite integer numbers α , κ . The function $\boldsymbol{\phi}$ can be seen as a transformation from the original state and input space to the flat output space. Often, it is possible to choose flat outputs that have a physical meaning, e.g., the conversion of a reactor, and that are a function of the states \mathbf{x} only (Adamy, 2014).

- (b) A backtransformation from the flat output and its derivatives to the original states \mathbf{x} and inputs \mathbf{u} can be found. Accordingly, the system states \mathbf{x} and inputs \mathbf{u} can be given as functions $\boldsymbol{\psi}_1$, $\boldsymbol{\psi}_2$ of the flat outputs $\boldsymbol{\xi}$, the production rate ρ , and a number of time derivatives of $\boldsymbol{\xi}$ and ρ :

$$\mathbf{x} = \boldsymbol{\psi}_1 \left(\boldsymbol{\xi}, \dot{\boldsymbol{\xi}}, \dots, \boldsymbol{\xi}^{(\beta-1)}, \rho, \dot{\rho}, \dots, \rho^{(\zeta-1)} \right) \quad (5b1)$$

$$\mathbf{u} = \boldsymbol{\psi}_2 \left(\boldsymbol{\xi}, \dot{\boldsymbol{\xi}}, \dots, \boldsymbol{\xi}^{(\beta)}, \rho, \dot{\rho}, \dots, \rho^{(\zeta)} \right) \quad (5b2)$$

with finite integer numbers β , ζ .

- (c) The components of $\boldsymbol{\xi}$ are differentially independent (Rothfuß, 1997). Consequently, they do not fulfill any differential equation:

$$\boldsymbol{\mu}(\boldsymbol{\xi}, \dot{\boldsymbol{\xi}}, \dots, \boldsymbol{\xi}^{(\beta)}) = \mathbf{0} \quad (5c)$$

Condition (5c) is satisfied if condition (5b) is satisfied, $\dim(\boldsymbol{\xi}) = \dim(\mathbf{u}) = m$, and $\text{rank} \left(\frac{\partial \mathbf{f}(\mathbf{x}, \mathbf{u}, \rho)}{\partial \mathbf{u}} \right) = m$, where m is the number of inputs (Rothfuß, 1997).

Note: To check conditions (5a) - (5c), a candidate for a flat output vector $\boldsymbol{\xi}$ is needed. We assume that such a candidate for a flat output vector $\boldsymbol{\xi}$ can be identified based on engineering intuition.

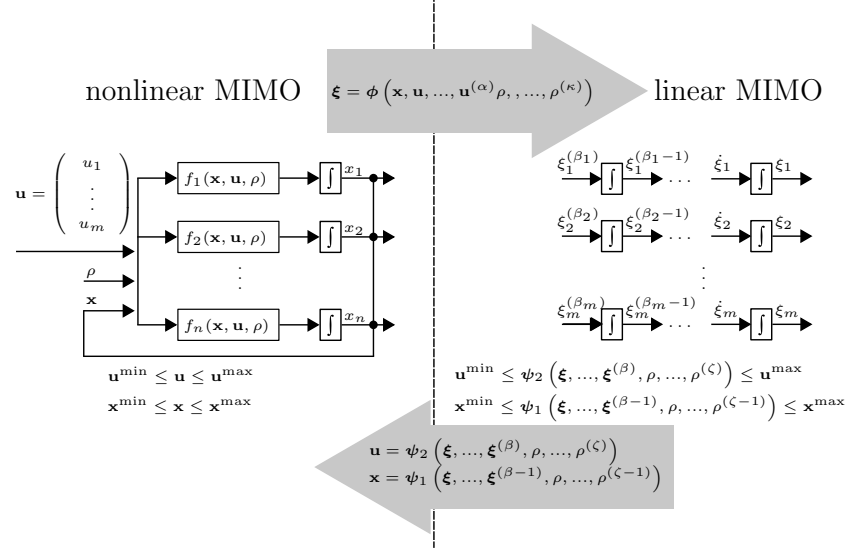


Fig. 2. Visualization of flatness-based coordinate transformation showing original nonlinear MIMO process model as introduced in assumption 1 (left), transformations ϕ, ψ_1, ψ_2 as introduced in assumption 3 (gray arrows), and linear MIMO process model in transformed coordinate space as introduced in assumption 3 (right).

4. The trajectory of the production rate ρ is determined by the scheduling optimization. Subsequently, the control input vector $\mathbf{u} \in \mathbb{R}^m$ is calculated by an underlying process control.

The flatness-based coordinate transformation is visualized in Figure 2. A nonlinear model with linear constraints is transformed into a linear model with nonlinear constraints. The number of control degrees of freedom is maintained: While, in the original model, the m inputs u_k ($k = 1, \dots, m$) are the degrees of freedom, in the linear model, the m highest time derivatives of the output components $\xi_k^{(\beta_k)}$ ($k = 1, \dots, m$) are the degrees of freedom (Adamy, 2014; Fliess et al., 1995). The number of time derivatives β_k can deviate between the flat output components ξ_k (Adamy, 2014; Fliess et al., 1995). In the linear model, the transformed state vector Ξ is formed by the outputs and their time derivatives (except for the highest time derivative):

$$\Xi = \left(\xi_1, \dots, \xi_1^{(\beta_1-1)}, \xi_2, \dots, \xi_2^{(\beta_2-1)}, \dots, \xi_m, \dots, \xi_m^{(\beta_m-1)} \right)^T \quad (6)$$

The dimension of the transformed state vector Ξ is greater or equal to the dimension of the original state vector \mathbf{x} (Adamy, 2014; Fliess et al., 1995). Consequently, the original nonlinear process model is converted to a linear model consisting of m integrator chains. In the linear model, every flat output ξ_k can be varied with a β_k -th order dynamic independently of the other flat outputs. Note that flatness is a sufficient condition for controllability of a nonlinear process (Adamy, 2014).

To ease notation in the following, we introduce the ramping state vector

$$\varphi = \left(\rho, \dot{\rho}, \dots, \rho^{(\delta-2)}, \rho^{(\delta-1)} \right)^T \quad (7)$$

and its time derivative

$$\dot{\varphi} = \left(\dot{\rho}, \rho^{(2)}, \dots, \rho^{(\delta-1)}, \nu \right)^T. \quad (8)$$

3.2 Approach

The steps to derive dynamic ramping constraints further discussed in the following subsections are summarized in Figure 3: First, a candidate for a flat output vector is selected based on two necessary flatness

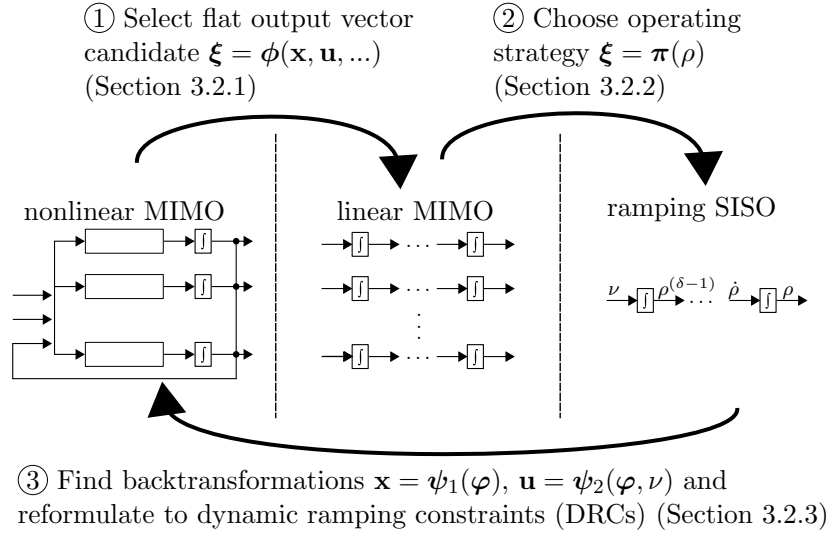


Fig. 3. Overview of steps to derive dynamic ramping constraints performed in the respective sections. For the nonlinear MIMO model and the linear MIMO model, all variable symbols are omitted for clarity as they are identical to Figure 2. The variables of the ramping SISO model are the production rate ρ , its derivatives $\dot{\rho}, \dots, \rho^{(\delta-1)}$, and the ramping degree of freedom ν .

conditions (Section 3.2.1). Assuming this candidate is, in fact, a flat output, the original nonlinear MIMO process model is transformed into a linear MIMO model (center of Figure 3). In this linear model, the m components of the flat output vector ξ_k are decoupled such that the outputs ξ_k can be controlled independently of each other by manipulating the degrees of freedom $\xi_k^{(\beta_k)}$ (Figure 2). However, a SISO model is needed for the dynamic ramping constraints where the production rate ρ is controlled by manipulating the ramping degree of freedom ν . Thus, second, the flat output components ξ_k are coupled by choosing an operating strategy $\pi(\rho)$ that defines every ξ_k as function of the production rate ρ (Section 3.2.2). This coupling reduces the number of degrees of freedom from m to one, leading to a significant model order reduction. Third, backtransformations are found from the ramping SISO model to the original nonlinear MIMO model, and thus flatness is proven (Section 3.2.3).

Based on the backtransformations and the ramping SISO model, the true nonlinear ramping limits are derived from the bounds on inputs \mathbf{u} and states \mathbf{x} . After approximating the true nonlinear limits with piecewise-affine functions, the dynamic ramping constraints are complete and the problem (P) can be solved as MILP.

3.2.1 Selection of flat output candidate and necessary flatness conditions

First, we propose to apply a necessary condition for flatness from literature based on a graph representation of the process (Schulze and Schenkendorf, 2020) to identify a candidate for the flat output vector ξ as $\phi(\mathbf{x}, \mathbf{u}, \dot{\mathbf{u}}, \dots, \mathbf{u}^{(\alpha)}, \rho, \dot{\rho}, \dots, \rho^{(\kappa)})$ (compare to condition 5a). As the second necessary condition for flatness, we propose setting up an equation system that implicitly defines the backtransformation ψ (compare to condition 5b) and check if this backtransformation equation system is structurally solvable.

For the graph representation, the process model is represented as a directed graph in which all states x_i and inputs u_k are represented as vertices v_{x_i} and v_{u_k} , respectively (Schulze and Schenkendorf, 2020). If $\frac{\partial f_i(\mathbf{x}, \mathbf{u})}{\partial x_j}$ is non-zero, there is an edge from vertex v_{x_j} to vertex v_{x_i} (Schulze and Schenkendorf, 2020). In other words: If a state x_j acts on the derivative of another state x_i , an edge is drawn from x_j to x_i . Similarly, an edge from input u_k to state x_i exists, if $\frac{\partial f_i(\mathbf{x}, \mathbf{u})}{\partial u_k}$ is non-zero. The necessary condition for a flat output vector ξ is that it must be possible to match the m output components ξ_i to the input

components u_i such that there are m input-output pairs with pairwise disjoint paths through the graph that cover all process states (Schulze and Schenkendorf, 2020). An illustrative example for this necessary condition is given in the Supplementary Information (SI).

As a starting point, the states which are typically controlled can be tested as flat output candidates. Typical states to be controlled are outlet stream compositions, final effluent temperature, or the process hold-up (Jogwar et al., 2009).

Once a flat output vector candidate is identified based on the graph representation as $\xi = \phi(\mathbf{x}, \mathbf{u}, \dot{\mathbf{u}}, \dots, \mathbf{u}^{(\alpha)}, \rho, \dot{\rho}, \dots, \rho^{(\kappa)})$, condition 4a is fulfilled. Further, the rank criterion needed for condition 4c can be checked easily. As a final step to show flatness, existence of the backtransformations ψ_1, ψ_2 that give states \mathbf{x} and inputs \mathbf{u} as functions of the flat output ξ and its time derivatives $\dot{\xi}, \dots, \xi^{(\beta)}$ needs to be shown (condition 4b). To obtain these backtransformations, a nonlinear system of equations needs to be developed with ξ and its derivatives $\dot{\xi}, \dots, \xi^{(\beta)}$ on the right-hand side and left-hand side functions including the wanted quantities: states \mathbf{x} , inputs \mathbf{u} , and potentially derivatives of inputs. To set up the backtransformation, we make use of the fact that ξ is given by $\phi(\mathbf{x}, \mathbf{u}, \dot{\mathbf{u}}, \dots, \mathbf{u}^{(\alpha)}, \rho, \dot{\rho}, \dots, \rho^{(\kappa)})$ and the derivatives of ξ can be given as functions of \mathbf{x} , inputs \mathbf{u} , and derivatives of inputs by means of the total differential. The equation system for the backtransformation needs to be square such that there are as many equations as there are unknown states, inputs, and derivatives of inputs. We propose to check if this nonlinear equation system is structurally solvable by conducting an analysis similar to the structural index analysis for differential-algebraic equation systems (Unger et al., 1995) commonly used in process systems engineering. An example is given in the SI.

3.2.2 Operating strategy

Under the assumption that the flat output candidate identified as discussed in Section 3.2.1 is, in fact, a flat output, the nonlinear model can be transformed into a linear model. This linear model is a MIMO model with m degrees of freedom $\xi_i^{(\beta_i)}$ and m outputs ξ_i (Figure 2). As discussed above, the linear MIMO is transferred to a SISO ramping model by coupling the flat output components. To this end, we insert an operating strategy that gives the value of every flat output as a function of the production rate ρ . This operating strategy differentiates between two possible types of flat output components: First, flat output components might have specifications that should be maintained constant, such as outlet stream compositions, final effluent temperature, and the process hold-up (Jogwar et al., 2009). Accordingly, the operating strategy is to hold such an output ξ_k constant at its nominal value such that $\xi_k = \xi_k^{\text{nom}}$ holds and thus all time derivatives are zero.

Second, flat output components may be unspecified. For instance, in our case study, one flat output component is a concentration for which no specifications are given. As every flat output component ξ_k corresponds to one control input, i.e., degree of freedom, u_k , if specifications are given for l outputs, and l is smaller than m , $m - l$ flat output components remain as degrees of freedom in steady-state. Thus, the $m - l$ free flat output component ξ_k can, in principle, be chosen to have any value in steady-state as long as no variable bounds are violated. To have the optimal steady-state operating points, we use a steady-state optimization to determine the optimal values ξ_k in advance as a function of the production rate ρ such that $\xi_k = \pi_k(\rho)$. For instance, the objective can be to find the steady-state operating points that minimize energy consumption. In our case study, we choose the flat output component such that the overall heat demand is minimal for steady-state points (Section 4).

The operating strategy $\pi_k(\rho)$ can be any nonlinear function. The only requirement is that the function $\pi_k(\rho)$ must be differentiable with respect to ρ sufficiently often so that all derivatives of ξ_k which are part of the backtransformation discussed in the previous section are defined by the total differential, e.g., $\dot{\xi}_k = \frac{\partial \pi_k(\rho)}{\partial \rho} \dot{\rho}$, $\xi_k^{(2)} = \frac{\partial \pi_k(\rho)}{\partial \rho} \rho^{(2)} + \frac{\partial^2 \pi_k(\rho)}{\partial \rho^2} \dot{\rho}^2$.

When all output components with specifications are maintained at their nominal values and a function $\pi_k(\rho)$ is chosen for all other output components, the operating strategy can be summarized as $\xi = \pi(\rho)$. Consequently, the flat output vector ξ and all relevant time derivatives $\xi, \dot{\xi}, \dots, \xi^{(\beta)}$ (compare to equation (5b)) are defined as function of the production rate ρ and a number of its time derivatives. The highest time derivative $\rho^{(\delta)}$ that occurs defines the order of the dynamic ramping constraint (DRC) and the ramping degree of freedom $\nu = \rho^{(\delta)}$. Consequently, the backtransformations ψ_1, ψ_2 discussed in the following only depend on the ramping state vector φ and the ramping degree of freedom ν .

3.2.3 Backtransformation and reformulation to dynamic ramping constraints

First, the flat output vector ξ and its time derivatives $\xi, \dot{\xi}, \dots, \xi^{(\beta)}$ are replaced in the nonlinear equation system for the backtransformation derived in Section 3.2.1. While ξ is replaced by $\pi(\rho)$, the derivatives are replaced by building the total differential of $\pi(\rho)$. Next, we solve the equation system to get $\mathbf{x} = \psi_1(\varphi)$ and $\mathbf{u} = \psi_2(\varphi, \nu)$. It is favorable to solve the equation system analytically. Still, it is not necessary to derive the functions ψ_1, ψ_2 analytically as they can also be evaluated numerically as long as their solution is unique. In this paper, we use the computer algebra package SymPy (Meurer et al., 2017) to obtain analytic functions ψ_1, ψ_2 . Note that it might not be possible to solve the system of equations because the graphical and structural criteria proposed in Section 3.2.1 are only necessary flatness conditions. In case the nonlinear system of equations cannot be solved, one can test other flat output candidates. If the functions ψ_1, ψ_2 are found, condition 3b is fulfilled, and flatness is shown at least locally on the subspace defined by the operating strategy.

This flat system constitutes one integrator chain with the degree of freedom ν that can be chosen arbitrarily at any point in time. Thus, mathematically, the production rate can be changed infinitely fast by choosing infinitely high values for ν . However, the real process control inputs \mathbf{u} are bounded by maximum and minimum values (assumption 3), and therefore, dynamic ramping constraints (DRCs) are needed to ensure that the real process inputs are maintained within bounds.

To get the dynamic ramping constraints (DRCs), we consider the input bounds row by row. For the k -th row, we get

$$u_k^{\min} \leq \psi_{2,k}(\rho, \dot{\rho}, \dots, \rho^{(\gamma)}) \leq u_k^{\max}, \quad (9)$$

where $\rho^{(\gamma)}$ is the highest time derivative needed to compute u_k . Equation (9) implicitly limits $\rho^{(\gamma)}$ for given $\rho, \dot{\rho}, \dots, \rho^{(\gamma-1)}$. These limits can be given as an explicit function if it is possible to symbolically invert $\psi_{2,k}$ for the derivative $\rho^{(\gamma)}_k$ and thus derive an analytic function θ of the production rate ρ , derivatives $\dot{\rho}, \dots, \rho^{(\gamma-1)}$, and the input u_k :

$$\rho^{(\gamma)}_k = \theta(\rho, \dot{\rho}, \dots, \rho^{(\gamma-1)}, u_k) \quad (10)$$

Inserting u_k^{\min}, u_k^{\max} into θ gives $\rho^{(\gamma)}_k^{\min}, \rho^{(\gamma)}_k^{\max}$. Alternatively, the limits can be derived numerically for given $\rho, \dot{\rho}, \dots, \rho^{(\gamma-1)}$ by sampling different values for $\rho^{(\gamma)}_k$ and evaluating if the resulting u_k is within the allowed range.

Note: Here, we discuss the case of one allowed region for $\rho^{(\gamma)}_k$ given by limits $\rho^{(\gamma)}_k^{\min}, \rho^{(\gamma)}_k^{\max}$. In principle, there could be two (or even more) non-connected allowed regions given by limits $\rho^{(\gamma)}_k^{\min,1}, \rho^{(\gamma)}_k^{\max,1}$ and $\rho^{(\gamma)}_k^{\min,2}, \rho^{(\gamma)}_k^{\max,2}$ with $\rho^{(\gamma)}_k^{\max,1} < \rho^{(\gamma)}_k^{\min,2}$, as $\psi_{2,k}$ is a general nonlinear function. In that case, one could either restrict the operating range to one of the two regions or introduce a binary variable that indicates which region is active. An illustrative example that can result in two allowed regions is given in the SI.

Bounds on a state x_k give an equation which has the same structure as Equation (9). Thus, constraints on states can be treated in the same way as constraints on inputs.

Finally, the nonlinear ramping limits need to be approximated by piecewise affine (PWA) functions. This approximation allows to explicitly balance the quality of the dynamic ramping constraints against the computational burden. In contrast to previous work (Baader et al., 2022a), there can more be several inputs and states limiting the same derivative of the production rate ρ for the MIMO case. Figure 4 shows an illustrative case with first-order ramping and two limiting inputs u_1, u_2 . The upper ramping limit is only determined by the maximum input u_1^{\max} as the upper limit in the flat system resulting from u_2^{\min} is always above the limit from u_1^{\max} . In contrast, the lower ramping limit is given by an intersection between the lower limits from u_1^{\min} and u_2^{\max} , respectively. If static ramping limits are chosen, a large amount of the feasible region needs to be cut off for the illustrative case in Figure 4 (horizontal dotted lines). In contrast, linear (dashed lines in Figure 4) and piecewise affine (dashed-dotted lines in Figure 4) limits allow to come closer to the true nonlinear limits and thus realize a larger flexibility range. For the lower ramping limit, piecewise affine limits can be realized without the addition of binary variables as the feasible region is convex. However, for the upper limit, the feasible region is non-convex and binary variables are needed, making the optimization more computationally challenging.

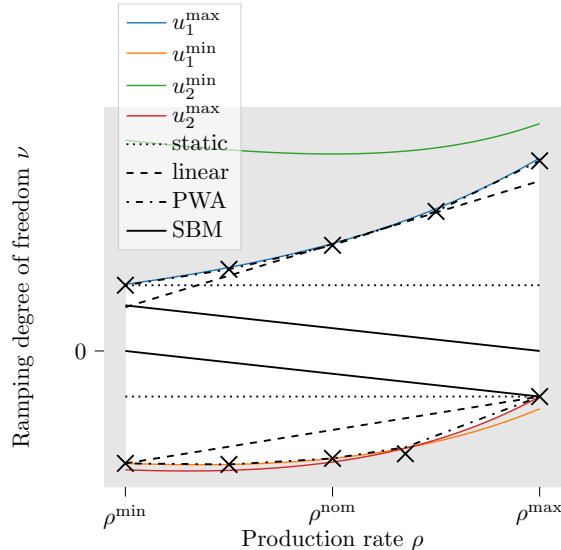


Fig. 4. Constraints for ramping degree of freedom ν as function of production rate ρ for an illustrative case with first-order ramping constraints and two limiting inputs u_1 , u_2 . For first-order ramping constraints, the ramping state vector φ is of dimension one and equal to the production rate ρ . Consequently, the limits on the ramping degree of freedom ν only depend on ρ . The true nonlinear limits caused by the minimum and maximum values of the two inputs u_1 , u_2 are compared to static limits (dotted), linear limits (dashed) and piecewise-affine (PWA) limits (dashed-dotted). Moreover, a linear scale-bridging model (SBM) is visualized (compare to discussion in Section 3.3)

As, in the general case, the limit functions $(\rho^{(\gamma)})^{\min}$, $(\rho^{(\gamma)})^{\max}$ are multivariate functions, multivariate regression methods, e.g., hinging hyperplanes (Breiman, 1993; Adeniran and Ferik, 2017; Kämper et al., 2021), convex region surrogates (Zhang et al., 2016; Schweidtmann et al., 2021), or artificial neural networks with ReLU activation functions (Grimstad and Andersson, 2019; Lueg et al., 2021), can be used to find piecewise-affine approximations.

3.3 Comparison to other approaches

Finally, we compare our approach to two other relevant approaches that integrate scheduling and control by considering a simplified version of the process dynamics in scheduling: scale-bridging models (Du et al., 2015) and data-driven closed-loop models (Kelley et al., 2018). The difference between the two alternative approaches is that scale-bridging models explicitly adapt the underlying control to linearize the closed-loop response (Du et al., 2015) while data-driven closed-loop models identify the response of the process to a change of the set-point ρ_{SP} from data (Dias and Ierapetritou, 2016; Diangelakis et al., 2017; Burnak et al., 2018; Pattison et al., 2016). Thus, data-driven closed-loop models, in general, identify a nonlinear closed-loop response, and scale-bridging models rely on a linearization performed by the underlying control. This linearization can be achieved by exact input-output linearization control (Du et al., 2015), scheduling-oriented model-predictive control (Baldea et al., 2015), or by a combination of a set-point filter and tracking control (Baader et al., 2022c). For first-order dynamics, the linearized closed-loop response reads

$$\rho + \tau \dot{\rho} = \rho_{SP} \quad (11)$$

In Equation (11), τ is a tunable time constant and ρ_{SP} is the set-point given to the underlying controller. That is, instead of the ramping degree of freedom ν , the set-point ρ_{SP} is the degree of freedom for the scheduling optimization. To compare the scale-bridging model to our dynamic ramping constraints, we

rearrange Equation (11) to calculate the maximum possible rate of change $\dot{\rho}^{\max}$ as a function of the maximum set-point ρ_{SP}^{\max} and the minimum rate of change $\dot{\rho}^{\min}$ as a function of the minimum set-point ρ_{SP}^{\min} :

$$\dot{\rho}^{\max} = \frac{1}{\tau}(\rho_{SP}^{\max} - \rho) \quad (12)$$

$$\dot{\rho}^{\min} = \frac{1}{\tau}(\rho_{SP}^{\min} - \rho) \quad (13)$$

The resulting limits are visualized in Figure 4 for the natural choice that the maximum set-point ρ_{SP}^{\max} equals the maximum production rate ρ^{\max} and the minimum set-point ρ_{SP}^{\min} equals the minimum production rate ρ^{\min} . The time constant τ is chosen such that the rate of change $\dot{\rho}$ demanded by the scale-bridging model is always within limits. The flexibility range for the scale-bridging model has a parallelogram shape dictated by Equations (12) and (13). Our dynamic ramping constraints can always match this parallelogram shape by linear ramping limits ν^{\min} , ν^{\max} . Additionally, dynamic ramping constraints also allow choosing linear limits with another shape or even piecewise affine limits. Thus dynamic ramping constraints can consistently perform at least as well as linear scale-bridging models. Moreover, our analysis could be used to rigorously choose the time constant τ of the scale-bridging model.

As stated above, data-driven closed-loop models identify a nonlinear closed-loop response. Still, if piecewise affine functions approximate nonlinearities, a MILP formulation is possible, see, e.g., Kelley et al. (2018) who derive an MILP formulation for Hammerstein-Wiener models. Thus, data-driven closed-loop models are an alternative to our dynamic ramping constraints; in particular, they are still applicable if no mechanistic process model is available or the process is not flat. If a flat mechanistic process model is available, there are two conceptual differences between dynamic ramping constraints and data-driven closed-loop models: First, dynamic ramping constraints have the theoretical advantage that they can be derived rigorously such that the feasibility of the optimized trajectory is guaranteed. Second, dynamic ramping constraints and data-driven closed-loop models lead to conceptually different trade-offs between computational burden and accuracy: While dynamic ramping constraints reduce the computational burden by reducing the accuracy of the ramping limits, data-driven closed-loop models reduce computational burden by reducing the accuracy of the model prediction. Thus, dynamic ramping constraints compromise on the feasible region, sacrificing flexibility, and data-driven closed-loop models compromise on the prediction of the process outputs, potentially leading to constraint violations or production deviating from the schedule.

4 Case study: Reactor-separator process with recycle

In this case study, we consider a reactor-separator process with recycle consisting of a continuous stirred tank reactor (CSTR) and a flash (Figure 5). The production rate ρ can be varied around its nominal value ρ^{nom} between $\rho^{\min} = 0.8\rho^{\text{nom}}$ and $\rho^{\max} = 1.2\rho^{\text{nom}}$ as long as the nominal production is reached on average over the considered time horizon. A raw material A reacts to the desired product B , which can further react to an undesired product C . The process has 6 differential states: the concentration of A , c_{A1} , the concentration of B , c_{B1} , and the temperature T_1 in the reactor (1) and the analog quantities c_{A2} , c_{B2} , T_2 , in the flash (2). Apart from the production rate ρ , there are four manipulated variables: the bottom stream F_B , the purge stream F_p , the heat flow to the reactor Q_1 , and the heat flow to the flash Q_2 . The process equations are modified from the textbook example by Christofides et al. (2011) where 2 CSTRs and a flash are considered. Though, also the original version (Christofides et al., 2011) fulfills our assumptions, we decided to modify the example to reduce the number of states from 9 to 6 to improve readability and clarity.

The model equations comprise component and energy balances given in the SI.

4.1 Selection of flat output candidate and necessary flatness conditions

A flat output candidate ξ must have 4 components as there are four control inputs. We first consider the three states of the flash c_{A2} , c_{B2} , and T_2 , as they determine the outlet stream, and we assume that

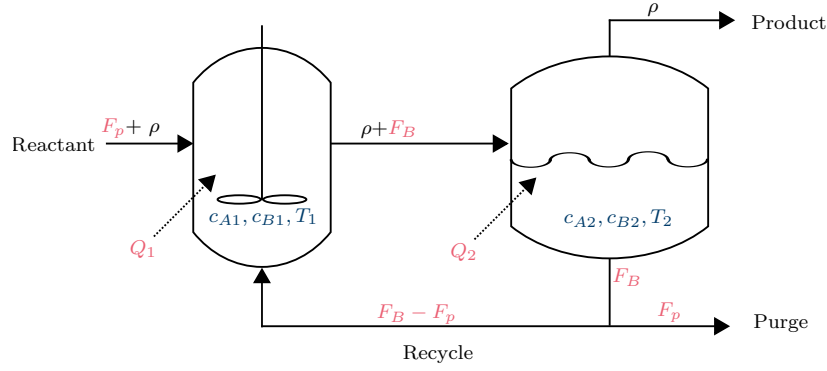


Fig. 5. Case study of reactor-separator process with recycle: States \mathbf{x} are the concentrations of component A and B, c_A , and c_B , respectively, and the temperature T in the reactor (1) and in the flash (2). Manipulated control inputs \mathbf{u} are the bottom stream F_B , the purge stream F_p , the heat input to the reactor Q_1 , and the heat input to the flash Q_2 . The scheduling degree of freedom is the production rate ρ . All other material flow rates are given as functions of F_B , F_p , and ρ , e.g., the reactant stream is equal to the purge F_p plus the production rate ρ as no accumulation of material occurs.

specifications for the outlet stream are given. As fourth output component, we choose the concentration c_{A1} based on the graph representation in Figure 6. The four input-output pairs $F_B - c_{A2}$, $F_p - c_{B2}$, $Q_2 - T_2$, $Q_1 - c_{A1}$ fulfill the necessary condition for a flat output (Figure 6).

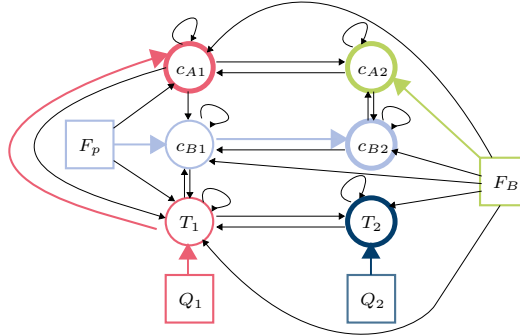


Fig. 6. Graph representation for the reactor-separator process with recycle (compare to Figure 5). The output $\xi = (c_{A2}, c_{B2}, T_2, c_{A1})^T$ fulfills the necessary condition for a flat output.

By differentiating the components of the output $\xi = (c_{A2}, c_{B2}, T_2, c_{A1})$ up to three times, we receive a structurally solvable system of equations (Table S3 in the SI).

4.2 Operating strategy

For the operating strategy, we assume that the composition and temperature of the product stream ρ must be maintained constant. Accordingly, $\xi_1 = c_{A2}$, $\xi_2 = c_{B2}$, $\xi_3 = T_2$ must be maintained at their nominal values $\xi_1^{\text{nom}} = 0.4539$, $\xi_2^{\text{nom}} = 0.4610$, $\xi_3^{\text{nom}} = 455K$. Thereby, the considered operating region is already significantly reduced.

As there are 4 control inputs, we can maintain the first three flat output components at their nominal values and still have one degree of freedom left. Consequently, an operating strategy for the fourth flat output $\xi_4 = c_{A1}$ can be chosen freely. In a steady-state optimization, we search for the steady-state operating points that minimize the total heating $Q_1 + Q_2$ and fix ξ_4 to be a function of the production rate $\xi_4 = \pi_4(\rho)$. Further details on this steady-state optimization are given in the SI.

Tab. 1. Structural dependency resulting from nonlinear transformation and operating strategy of states and inputs on the production rate ρ and its time derivatives $\dot{\rho}$ and ν ($= \rho^{(2)}$). States which are held constant are marked with a star (*).

		ρ	$\dot{\rho}$	ν
states:	c_{A1}	x		
	c_{B1}	x		
	T_1	x	x	
	c_{A2}^*			
	c_{B2}^*			
	T_2^*			
inputs:	F_B	x		
	F_p	x	x	
	Q_1	x	x	x
	Q_2	x	x	

4.3 Reformulation to dynamic ramping constraints

After inserting the operating strategy defined in Section 4.2, we solve the nonlinear backtransformation equation system. To this end, we use the computer algebra package SymPy (Meurer et al., 2017) to find explicit algebraic expressions for all states and inputs, except for the temperature T_1 . The temperature T_1 has to be determined numerically because the two reaction terms in the differential Equation (S9) lead to an equation of the form

$$0 = b_0 + b_1 e^{-\frac{E_1}{RT_1}} + b_2 e^{-\frac{E_2}{RT_1}}, \quad (14)$$

with parameters b_0, b_1, b_2 . The implicit Equation (14) has a unique solution for the temperature, as the exponential functions are monotonic. The numerical solution of Equation (14) is found using the python package SciPy (Virtanen et al., 2020).

Table 1 provides the structural dependency of the states and inputs on the production rate ρ and its time derivatives $\dot{\rho}$ and ν ($= \rho^{(2)}$). The highest time derivative of the production rate that appears is two. Therefore, the ramping degree of freedom ν is equal to $\rho^{(2)}$. More detailed information about the reformulations is given in the SI.

For the dynamic ramping constraints, it has to be analyzed which state and input bounds limit the time derivatives of the production rate ρ . States and inputs that are either held constant or exclusively depend on the production rate ρ do not need to be checked because it is already known from the steady-state optimization that these variables take feasible values for all considered production rates. Consequently, the variables $c_{A,1}, c_{B,1}, c_{A,2}, c_{B,2}, T_2, F_B$ do not influence the dynamic ramping constraints (compare to Table 1).

The variables T_1, F_p, Q_2 depend on ρ and $\dot{\rho}$ but not on the second time derivative ν . Accordingly, the bounds of these variables limit the first time derivative $\dot{\rho}$. In Figure 7, the limits on $\dot{\rho}$ resulting from variable bounds are shown over the production rate ρ . The calculation of these limits is explained in the SI. While the lower limit on $\dot{\rho}$ results from the bound F_p^{\min} , the upper limit is given by F_p^{\max} for small production rates and by Q_2^{\min} for large production rates. Graphically, we choose conservative linear functions for the limits $\dot{\rho}^{\min}(\rho) = a_0^{\min} + a_1^{\min}\rho$, $\dot{\rho}^{\max}(\rho) = a_0^{\max} + a_1^{\max}\rho$ with parameters $a_0^{\min}, a_1^{\min}, a_0^{\max}, a_1^{\max}$ (compare to (DRCb)).

The heating input Q_1 is the only variable that depends on the ramping degree of freedom ν . We choose piecewise affine limits $\nu_{\text{PWA}}^{\min}(\rho, \dot{\rho})$, $\nu_{\text{PWA}}^{\max}(\rho, \dot{\rho})$ (compare to DRCd) which cover 95% of the feasible area. Further details are given in the SI.

With the limits on ν , the second-order dynamic ramping constraints are completely parameterized

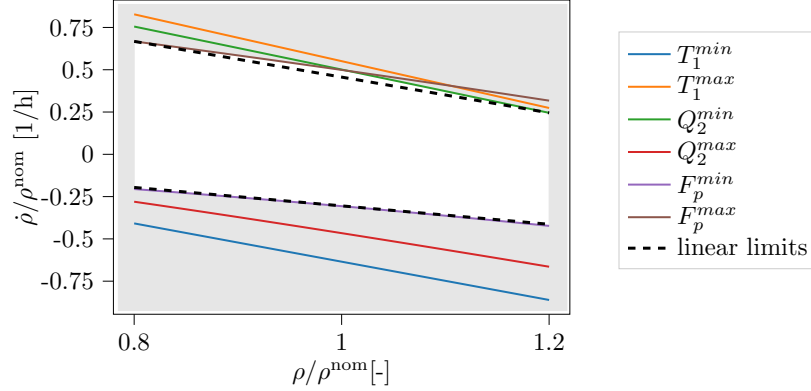


Fig. 7. Limits on the scaled time derivative of the production rate $\dot{\rho}$ over the scaled production rate ρ resulting from the minimum (min) and maximum (max) values of the state T_1 and the inputs F_p , Q_2 .

and have the form:

$$\rho^{(2)} = \nu \quad (15)$$

$$a_0^{\min} + a_1^{\min} \rho \leq \dot{\rho} \leq a_0^{\max} + a_1^{\max} \rho \quad (16)$$

$$\nu_{\text{PWA}}^{\min}(\rho, \dot{\rho}) \leq \nu \leq \nu_{\text{PWA}}^{\max}(\rho, \dot{\rho}) \quad (17)$$

4.4 Investigation 1: Ramp optimizations

To illustrate the ramping behavior with the derived dynamic ramping constraints, we perform two as-fast-as-possible ramp optimizations shown in Figure 8. The ramp-up from minimum production rate to maximum production rate takes 1.3 hours, and the corresponding ramp-down takes 3.1 hours. The ramp-up is first constrained by the acceleration, i.e., the bounds on ν , and then by the speed, i.e., the bounds on $\dot{\rho}$. In contrary, the ramp-down is always constrained by the bounds on ν .

To visualize such an optimized ramp on the full-order process model, we simulate the ramp-up by using the optimized production rate trajectory (left part of Figure 8) as input to a simulation and calculate the control inputs \mathbf{u} using the backtransformation function $\mathbf{u} = \psi_2(\rho, \dot{\rho}, \nu)$ derived above. While the first three flat output components c_{A2}, c_{B2}, T_2 are maintained at their nominal values, the fourth output component c_{A1} follows the function of the production rate $c_{A1} = \pi_4(\rho)$ specified in the operating strategy (Figure 9). All other states and inputs are within their respective bounds. Moreover, in the first half hour, when the ramp-up is limited by the limit on the acceleration ν^{\max} (compare to Figure 8, left), Q_1 is close to its maximum value (Figure 9) because the upper limit of ν^{\max} is derived from Q_1^{\max} . However, Q_1 does not reach its maximum value due to the conservative piecewise affine approximation. During the second half hour, the ramp-up is limited by the maximum speed $\dot{\rho}^{\max}$ (compare to Figure 8, left) and thus the control input Q_2 , which limits the speed for high production rates ρ (compare to Figure 7), is close to its bounds (Figure 9). Here, Q_2 comes very close to its bound as the conservative approximation of the ramping limit on $\dot{\rho}$ is very close to the true nonlinear limit (Figure 7). Finally, at hour 1.25, the acceleration ν touches the lower limit ν^{\min} (Figure 8) and the input Q_1 reaches its lower limit Q_1^{\min} (Figure 9).

Ramp optimization and corresponding simulation show that even though the dynamic ramping constraints are formed by linear and piecewise affine equations, they can capture dynamics that are significantly more complex than traditional static first-order ramps. Moreover, the original process model with 6 states and 5 degrees of freedom is reduced to a dynamic ramping constraint with only 2 states, i.e., ρ , $\dot{\rho}$, and one degree of freedom ν . Accordingly, coupling the flat outputs to the production rate reduces the model size and thus simplifies optimization.

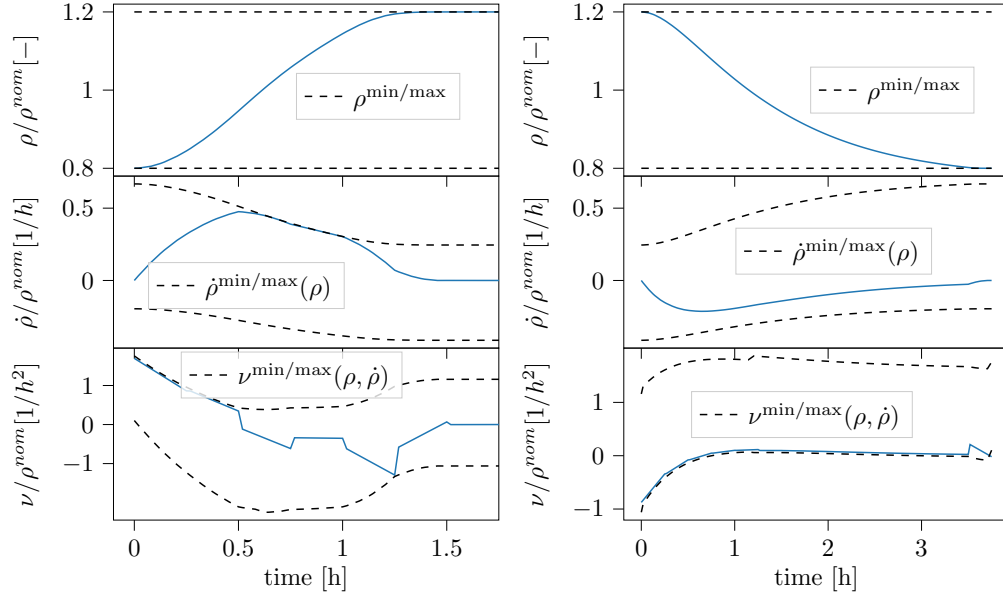


Fig. 8. Production rate ρ , its first time derivative $\dot{\rho}$, and ramping degree of freedom ν for an as-fast-as-possible ramp up (left) and an as-fast-as-possible ramp down (right) together with their bounds. The bounds of $\dot{\rho}$ are functions of ρ and the bounds of ν are functions of $\rho, \dot{\rho}$. The ramping degree of freedom ν is discretized to be piece-wise linear.

4.5 Investigation 2: Demand response application

To demonstrate the dynamic ramping constraints in a DR application, the flexible process is considered together with a multi-energy system and additional non-flexible heat and electricity demands (Figure 10). We consider an energy system based on [Sass et al. \(2020\)](#). However, instead of one combined heat and power plant (CHP) and one boiler (B), we extended the system to 4 CHPs and 2 boilers to study a larger energy system with more discrete on/off-decisions. Additionally, electricity can be bought from and sold to the grid for the day-ahead price that may change hourly. The details about the multi-energy system and the derivation of the optimization problem (P) are given in the SI.

The optimization problem (P) is formulated using pyomo ([Hart et al., 2017, 2011](#)) and discretized using the extension pyomo.dae ([Nicholson et al., 2018](#)). We apply discretization by orthogonal collocation on finite elements with 2 elements per hour and 3 collocation points per element. This discretization was found to be sufficiently accurate in preliminary calculations. Overall, we have 144 discretization points over the 24 hour time horizon. The discretized problem has 5,559 continuous variables. For the binary variables, we use a time discretization of one hour to match the time step of electricity prices. There are 6 binaries per hour for the on/off-decision of energy system units and 3 binaries per hour for the piecewise affine limits on the ramping degree of freedom ν and the piecewise affine energy demand model (more details in the SI). Thus, the final MILP problem has $9 \times 24 = 216$ binary variables.

The optimization problem is solved using gurobi version 9.5.2 ([Gurobi Optimization, LLC, 2021](#)). As [Harjunoski et al. \(2014\)](#) state that the maximum acceptable optimization runtime for scheduling problems is typically between 5 and 20 minutes, we set the maximum optimization runtime to 5 minutes. All calculations are performed on a Windows 11 machine with an Intel(R) Core(TM) i7-1165G7 CPU and 16 GB RAM.

First, the energy system operation is optimized without accounting for the energy demand of the flexible process to obtain the energy costs of the inflexible demands only. Second, the operation of the energy system is optimized with the flexible process operating in steady-state such that the demand of the flexible process is constant (compare to Figure 11, right). Third, the DR optimization is performed

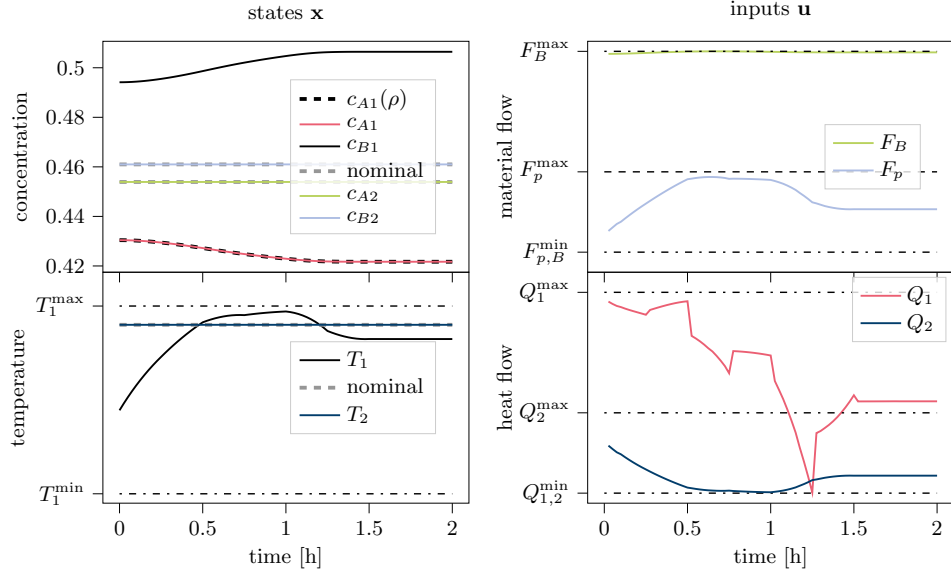


Fig. 9. Simulation result of ramp-up optimization (Figure 10, left) on the full-order process model showing states $\mathbf{x} = (c_{A1}, c_{B1}, T_1, c_{A2}, c_{B2}, T_2)^T$ (left), and control inputs $\mathbf{u} = (F_B, F_p, Q_1, Q_2)^T$ (right). Minimum (min) and maximum (max) values are shown in dashed-dotted lines. The nominal values of the flat output components c_{A2}, c_{B2}, T_2 and the operating strategy $\pi_4(\rho)$ for the flat output component c_{A1} are shown in dashed lines.

using dynamic ramping constraints (compare to Figure 11, left).

The DR operation of the process reduces the total energy costs by 4.6 % compared to steady-state operation. Considering only the energy costs associated with the flexible process, the cost reduction through demand response is 9.8 %.

In the resulting operation, two types of periods can be distinguished: In times of low electricity prices, heat is preferably produced by the boilers, and electricity is bought from the grid (hours 13 - 18). In times of high electricity prices, heat is preferable provided by the CHPs, and excess electricity is sold to the grid (hours 1-12, 19-24). The DR case reduces costs due to two reasons: First, the boilers are operated less. Instead of 12 hours, the boilers are only active in 10 hours (Figure 11). The amount of heat provided by the boilers is reduced by 2 %. Second, the heat demand of the flexible process and, therefore, the electricity production of the CHPs is shifted from hours of low prices to hours with higher prices (Figures 11). For instance, the heat demand is lower in hour 15 and higher in hour 5. Consequently, the derived dynamic ramping constraints allow to reduce costs substantially compared to steady-state process operation.

The optimization problem terminates after a maximum runtime of 5 minutes that we set following Harjunkski et al. (2014). The remaining optimality gap is 3.9 %. As a further comparison, we simplify the bounds of the ramping degree of freedom ν in Equation (17) from piecewise affine to purely linear functions. These linear functions only cover 80% instead of 95% of the feasible area for ν (compare to Section 4.2). With these linear limits ν_{lin}^{\min} , ν_{lin}^{\max} , we receive very similar results compared to those previously obtained with the piecewise affine limits: While the cost reductions achieved with the linear limits slightly improve to 4.7% instead of 4.6%, the remaining optimality gap slightly worsens to 4.2% instead of 3.9%. That is, with purely linear dynamic ramping constraints, we find a comparable near-optimal solution with a comparable optimality gap. Overall, even if the on/off-status of 6 energy system units has to be optimized simultaneously with the process operation, the optimization provides a schedule achieving substantial cost reductions within this maximum optimization runtime of 5 minutes.

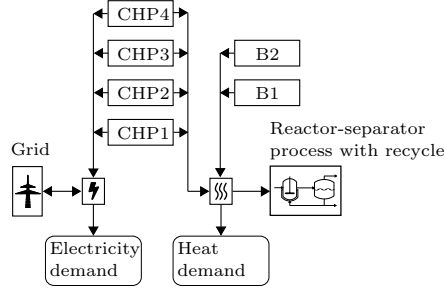


Fig. 10. Multi-energy system and reactor-separator process with recycle: The flexible process as well as additional non-flexible heat and electricity demands are supplied by an multi-energy system, consisting of 4 combined heat and power plants (CHP1-CHP4) and 2 boilers (B1, B2). Moreover, electricity can be exchanged with the grid.

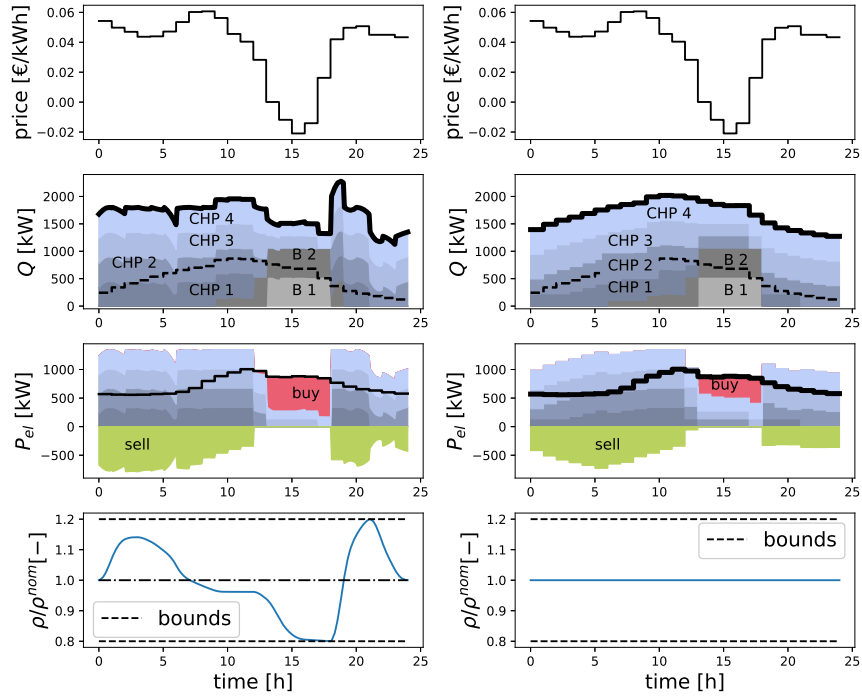


Fig. 11. Resulting schedule for the flexible process performing demand response (left) and the flexible process being operated in steady-state (right). Top: electricity price. Second row: heat supplied by the 4 combined heat and power plants (CHP1 - CHP4) and the two boilers (B1, B2). The inflexible heat demand is shown as dashed black line and the total heat demand as bold black line. Third row: Electricity generated by CHP1 - CHP4, sold electricity to the grid, and electricity bought from the grid. The inflexible electricity demand is shown as black line. Bottom: Production rate ρ .

5 Discussion

In this section, we discuss possible adaptations and limitations of our approach.

Throughout this paper, we assume that the production rate ρ is a degree of freedom (compare to assumptions in Section 3.1). However, the method can be adapted to cases where the production rate is not a degree of freedom but a component of the flat output vector ξ_k . For instance, if the flow rate of the

product stream would be hydraulically driven by a filling level h_{fill} , the production rate would be given as part of the flat output by a function of h_{fill} . In such cases, the production rate cannot be controlled directly but only through manipulating the corresponding input u_k . For instance, the filling level h_{fill} could be controlled by manipulating the feedflow of the corresponding unit.

In our operating strategy discussed in Section 3.2.2, all flat output components without given specifications are coupled to the production rate. This coupling reduces the dimensionality of the model. Instead of m flat outputs and their derivatives, only the production rate and its derivatives are variables in the optimization problem. Consequently, there are δ states and one degree of freedom. This dimensionality reduction strongly reduces the computational complexity of the optimization problem. Still, coupling all flat outputs with the production rate might be unfavorable in cases where some flat outputs can only be changed much slower than the production rate. In such cases, the outputs without specifications could be kept as independent integrator chains in the ramping model (right part in Figure 3). In our case study, the concentration c_{A1} , which is the fourth flat output component, could be uncoupled such that there are two integrator chains in the ramping model: one for the production rate ρ and one for the concentration c_{A1} . Consequently, dynamic ramping constraints need to be derived for both integrator chains. While this uncoupled version makes the ramping model computationally more challenging, it is also more flexible and thus might enable higher profits in some cases. An extreme example is electrolyzers that can often adapt their production rate rapidly but have slow temperature dynamics (Simkoff and Baldea, 2020; Flamm et al., 2021). Thus, for electrolyzers, it is not favorable to couple the temperature with the production rate. Instead, we have shown recently in a conference paper that it is favorable to keep both production rate and temperature as degrees of freedom and formulate dynamic ramping constraints on the temperature (Baader et al., 2022b).

Conceptually, the electrolyzer example (Baader et al., 2022b) also shows that it is possible to consider two scheduling-relevant variables at a time. Especially, our approach based on dynamic ramping constraints could be applied to the case of processes with two production rates ρ_1 and ρ_2 , where the process model from Equation (4) changes to $\dot{\mathbf{x}} = \mathbf{f}(\mathbf{x}, \mathbf{u}, \rho_1, \rho_2)$. In that case, there would be two ramping state vectors $\boldsymbol{\varphi}_1$ and $\boldsymbol{\varphi}_2$ and two ramping degrees of freedom ν_1 and ν_2 . In general, the ramping degrees of freedom ν_1, ν_2 are limited by both ramping state vectors $\boldsymbol{\varphi}_1, \boldsymbol{\varphi}_2$ and also influence each other. Thus, the ramping limits read:

$$\nu_1^{\min}(\boldsymbol{\varphi}_1, \boldsymbol{\varphi}_2, \nu_2) \leq \nu_1 \leq \nu_1^{\max}(\boldsymbol{\varphi}_1, \boldsymbol{\varphi}_2, \nu_2) \quad (18)$$

$$\nu_2^{\min}(\boldsymbol{\varphi}_1, \boldsymbol{\varphi}_2, \nu_1) \leq \nu_2 \leq \nu_2^{\max}(\boldsymbol{\varphi}_1, \boldsymbol{\varphi}_2, \nu_1) \quad (19)$$

In principle, our dynamic ramping approach can also be applied to more than two scheduling-relevant variables. However, increasing the number of scheduling-relevant variables also increases the number of arguments entering the functions $\nu_i^{\min}(\cdot), \nu_i^{\max}(\cdot)$. Thus, a piecewise affine approximation of the ramping limits $\nu_i^{\min}(\cdot), \nu_i^{\max}(\cdot)$ might require many binaries and lead to a high computational burden.

The present work focuses on demand response applications where the production rate ρ is the main scheduling-relevant variable. However, it is straightforward to adapt the approach to cases where a different variable is scheduling-relevant. For example, in multi-product processes, the concentration may be varied to yield different products. Thus, the scheduling needs to account for the dynamics of the concentration during product transitions (Flores-Tlacuahuac and Grossmann, 2006; Baader et al., 2022c). Our approach can be transferred to such a multi-product process if the production rate ρ is replaced by the concentration.

The main limitation of our approach is the assumption of a flat process model. For non-flat process models, the ramping limits could still be derived as functions of all process states \mathbf{x} . However, it is not possible to find the coordinate transformation from the process states \mathbf{x} to a transformed state vector Ξ as defined in Equation (6), and thus, the ramping limits cannot be given as functions of the ramping state vector $\boldsymbol{\varphi}$ only. Hence, an extension to non-flat processes would be partly heuristic as the state vector \mathbf{x} in the ramping limits would have to be approximated based on the ramping state $\boldsymbol{\varphi}$.

Another limitation of this work is that solving the equation system to derive the backtransformation requires a lot of manual effort, even though a computer algebra system is used as support. It is an open question to what extent our approach can be automated to enable the analysis of large-scale processes. Still, we do not consider this to be a significant restriction of our work as processes fulfilling our flatness

assumption usually do not have too many states (Oldenburg and Marquardt, 2002): As inputs must be matched to outputs such that all states are covered (compare to the necessary graphical condition, e.g., Figure 6), processes having much more states than inputs are usually not flat. Thus, our method will likely not be applicable to large-scale process models with hundreds of states. However, our approach seems applicable for flat process models with a number of states in the low double-digit range. As stated at the beginning of Section 4, we only reduced the textbook example by Christofides et al. (2011) from 9 states to 6 to ease the readability of the paper. Still, in a previous version, we considered the original version with 9 states and could find the inverse transformation easily using computer algebra. In future work, our approach could be coupled with model-order reduction approaches that derive a low-order representation of the process dynamics for the slow time scale (Baldea and Daoutidis, 2012). Even if the full-scale process model is not flat, the low-order dynamics relevant for scheduling optimization might be.

6 Conclusion

Dynamic ramping constraints simplify the simultaneous demand response scheduling optimization of production processes and their energy systems compared to an optimization considering the full-order process model. Still, dynamic ramping constraints can capture more flexibility than traditional static ramping constraints as they allow high-order dynamics and non-constant ramp limits. In this paper, we extend our method to rigorously derive dynamic ramping constraints from input-state linearizable single-input single-output (SISO) processes (Baader et al., 2022a) to flat multi-input multi-output (MIMO) processes. In the MIMO case, dynamic ramping constraints reduce the problem dimensionality by coupling all flat outputs with the production rate. In our case study, a system with 6 states and 5 degrees of freedom is reduced to 2 states and one degree of freedom. Additionally, we demonstrate that an operational strategy can be chosen for flat outputs such that the steady-state production points are optimal, e.g., with respect to energy consumption.

Our case study demonstrates that dynamic ramping constraints allow for finding DR schedules for flexible processes and multi-energy systems that substantially reduce energy costs compared to a steady-state operation. Even though discrete on/off-decisions in the multi-energy system add to the computational complexity, the problem can be solved within the time limit for online scheduling.

Overall, dynamic ramping constraints allow bridging the gap between nonlinear process models and simplified process representations suitable for real-time scheduling optimization.

Author contributions

Florian J. Baader (FB): Conceptualization, Methodology, Software, Investigation, Validation, Visualization, Writing - original draft. **Philipp Althaus (PA)**: Conceptualization, Writing – review & editing. **André Bardow (AB)**: Funding acquisition, Conceptualization, Supervision, Writing – review & editing. **Manuel Dahmen (MD)**: Conceptualization, Supervision, Writing – review & editing.

Declaration of Competing Interest

We have no conflict of interest.

Acknowledgements

This work was supported by the Helmholtz Association, Germany under the Joint Initiative ‘Energy System Integration’. AB and FB also received support from the Swiss Federal Office of Energy, Switzerland through the project ‘SWEET PATHFINDER’.

Nomenclature

Abbreviations

CHP	combined heat and power plant
CSTR	continuous stirred tank reactor
DR	demand response
DRC	dynamic ramping constraint
MIDO	mixed-integer dynamic optimization
MILP	mixed-integer linear program
MIMO	multi-input multi-output
MINLP	mixed-integer nonlinear program
SISO	single-input single-output

Greek symbols

α	integer number (compare to assumption 3a)
α_K	relative volatility of component K
β	integer number (compare to assumption 3b)
γ	integer number (compare to assumption 3b)
δ	order of dynamic ramping constraint
ζ	integer number
κ	integer number (compare to assumption 3a)
ν	ramping degree of freedom
Ξ	transformed state vector
ξ	flat output
π	operating strategy
ρ	production rate
ϱ_F	density
Φ	objective
ϕ	transformation to flat output
φ	ramping state vector
ψ	backtransformation from flat output

Latin symbols

a	coefficient
b	parameter
C	coverage
C_p	heat capacity
c	concentration
E	activation energy
F	flow rate
f	nonlinear function
H	enthalpy
k	reaction constant
m	number of control inputs
n	number of states
P	power
Q	heat flow
R	gas constant
T	temperature
t	time
u	control input

V	volume
v	vertex
x	state
z	binary variable

Subscripts

0	feed
1	reactor
2	flash
A	component A
B	component B or bottom
C	component C
dem	demand
el	electric
f	final time
p	purge
s	steady-state
V	vaporization

Superscripts

max	maximum
min	minimum
nom	nominal

Bibliography

- Adamson, R., Hobbs, M., Silcock, A., and Willis, M. J. (2017). Integrated real-time production scheduling of a multiple cryogenic air separation unit and compressor plant. *Computers & Chemical Engineering*, 104:25–37.
- Adamy, J. (2014). *Nichtlineare Systeme und Regelungen*. Springer Vieweg.
- Adeniran, A. A. and Ferik, S. E. (2017). Modeling and identification of nonlinear systems: A review of the multimodel approach—part 1. *IEEE Transactions on Systems, Man, and Cybernetics: Systems*, 47(7):1149–1159.
- Baader, F. J., Althaus, P., Bardow, A., and Dahmen, M. (2022a). Dynamic ramping for demand response of processes and energy systems based on exact linearization. *Journal of Process Control*, 118:218–230.
- Baader, F. J., Bardow, A., and Dahmen, M. (2022b). MILP formulation for dynamic demand response of electrolyzers. In Yamashita, Y. and Kano, M., editors, *14th International Symposium on Process Systems Engineering*, volume 49 of *Computer Aided Chemical Engineering*, pages 391–396. Elsevier.
- Baader, F. J., Bardow, A., and Dahmen, M. (2022c). Simultaneous mixed-integer dynamic scheduling of processes and their energy systems. *AIChE Journal*, page e17741.
- Baldea, M. and Daoutidis, P. (2012). *Dynamics and Nonlinear Control of Integrated Process Systems*. Cambridge Series in Chemical Engineering. Cambridge University Press.
- Baldea, M., Du, J., Park, J., and Harjunkski, I. (2015). Integrated production scheduling and model predictive control of continuous processes. *AIChE Journal*, 61(12):4179–4190.
- Baldea, M. and Harjunkski, I. (2014). Integrated production scheduling and process control: A systematic review. *Computers & Chemical Engineering*, 71:377–390.
- Biegler, L. T. (2010). *Nonlinear Programming: Concepts, Algorithms, and Applications to Chemical Processes*. Society for Industrial and Applied Mathematics.
- Breiman, L. (1993). Hinging hyperplanes for regression, classification, and function approximation. *IEEE Transactions on Information Theory*, 39(3):999–1013.
- Burnak, B., Katz, J., Dangelakis, N. A., and Pistikopoulos, E. N. (2018). Simultaneous process scheduling and control: A multiparametric programming-based approach. *Industrial & Engineering Chemistry Research*, 57(11):3963–3976.
- Carrion, M. and Arroyo, J. M. (2006). A computationally efficient mixed-integer linear formulation for the thermal unit commitment problem. *IEEE Transactions on Power Systems*, 21(3):1371–1378.
- Christofides, P. D., Liu, J., and La Muñoz de Peña, D. (2011). *Networked and Distributed Predictive Control*. Springer London, London.
- Dangelakis, N. A., Burnak, B., and Pistikopoulos, E. N. (2017). A multi-parametric programming approach for the simultaneous process scheduling and control application to a domestic cogeneration unit. Foundations of Computer Aided Process Operations/Chemical Process Control (FO-CAPO/CPC) https://folk.ntnu.no/skoge/prost/proceedings/focapo-cpc-2017/FOCAP0-CPC%202017%20Contributed%20Papers/72_FOCAP0_Contributed.pdf (accessed 06 January 2022).
- Dias, L. S. and Ierapetritou, M. G. (2016). Integration of scheduling and control under uncertainties: Review and challenges. *Chemical Engineering Research and Design*, 116:98–113.
- Du, J., Park, J., Harjunkski, I., and Baldea, M. (2015). A time scale-bridging approach for integrating production scheduling and process control. *Computers & Chemical Engineering*, 79:59–69.

- Flamm, B., Peter, C., Büchi, F. N., and Lygeros, J. (2021). Electrolyzer modeling and real-time control for optimized production of hydrogen gas. *Applied Energy*, 281:116031.
- Fliess, M., Lévine, J., Martin, P., and Rouchon, P. (1995). Flatness and defect of non-linear systems: Introductory theory and examples. *International Journal of Control*, 61:13–27.
- Flores-Tlacuahuac, A. and Grossmann, I. E. (2006). Simultaneous cyclic scheduling and control of a multiproduct CSTR. *Industrial & Engineering Chemistry Research*, 45(20):6698–6712.
- Grimstad, B. and Andersson, H. (2019). ReLu networks as surrogate models in mixed-integer linear programs. *Computers & Chemical Engineering*, 131:106580.
- Gurobi Optimization, LLC (2021). Gurobi optimizer reference manual. <http://www.gurobi.com> (accessed 09 February 2021).
- Harjunkski, I., Maravelias, C. T., Bongers, P., Castro, P. M., Engell, S., Grossmann, I. E., Hooker, J., Méndez, C., Sand, G., and Wassick, J. (2014). Scope for industrial applications of production scheduling models and solution methods. *Computers & Chemical Engineering*, 62:161–193.
- Hart, W. E., Laird, C. D., Watson, J.-P., Woodruff, D. L., Hackebeil, G. A., Nicholson, B. L., and Sirola, J. D. (2017). *Pyomo—Optimization modeling in Python*, volume 67. Springer Science & Business Media, second edition.
- Hart, W. E., Watson, J.-P., and Woodruff, D. L. (2011). Pyomo: Modeling and solving mathematical programs in python. *Mathematical Programming Computation*, 3(3):219–260.
- Hoffmann, C., Hübner, J., Klauke, F., Milojević, N., Müller, R., Neumann, M., Weigert, J., Esche, E., Hofmann, M., Repke, J.-U., Schomäcker, R., Strasser, P., and Tsatsaronis, G. (2021). Assessing the realizable flexibility potential of electrochemical processes. *Industrial & Engineering Chemistry Research*, 60(37):13637–13660.
- Jogwar, S. S., Baldea, M., and Daoutidis, P. (2009). Dynamics and control of process networks with large energy recycle. *Industrial & Engineering Chemistry Research*, 48(13):6087–6097.
- Kämper, A., Holtwerth, A., Leenders, L., and Bardow, A. (2021). Automog 3d: Automated data-driven model generation of multi-energy systems using hinging hyperplanes. *Frontiers in Energy Research*, 9:430.
- Kelley, M. T., Pattison, R. C., Baldick, R., and Baldea, M. (2018). An efficient MILP framework for integrating nonlinear process dynamics and control in optimal production scheduling calculations. *Computers & Chemical Engineering*, 110:35–52.
- Leenders, L., Bahl, B., Hennen, M., and Bardow, A. (2019). Coordinating scheduling of production and utility system using a stackelberg game. *Energy*, 175:1283–1295.
- Lueg, L., Grimstad, B., Mitsos, A., and Schweidtmann, A. M. (2021). reluMIP: Open source tool for MILP optimization of ReLu neural networks.
- Meurer, A., Smith, C. P., Paprocki, M., Čertík, O., Kirpichev, S. B., Rocklin, M., Kumar, A., Ivanov, S., Moore, J. K., Singh, S., Rathnayake, T., Vig, S., Granger, B. E., Muller, R. P., Bonazzi, F., Gupta, H., Vats, S., Johansson, F., Pedregosa, F., Curry, M. J., Terrel, A. R., Roučka, Š., Saboo, A., Fernando, I., Kulal, S., Cimrman, R., and Scopatz, A. (2017). SymPy: symbolic computing in Python. *PeerJ Comput. Sci.*, 3:e103.
- Mitra, S., Grossmann, I. E., Pinto, J. M., and Arora, N. (2012). Optimal production planning under time-sensitive electricity prices for continuous power-intensive processes. *Computers & Chemical Engineering*, 38:171–184.

- Nicholson, B., Siirola, J. D., Watson, J.-P., Zavala, V. M., and Biegler, L. T. (2018). Pyomo.dae: A modeling and automatic discretization framework for optimization with differential and algebraic equations. *Mathematical Programming Computation*, 10(2):187–223.
- Oldenburg, J. and Marquardt, W. (2002). Flatness and higher order differential model representations in dynamic optimization. *Computers & Chemical Engineering*, 26(3):385–400.
- Pattison, R. C., Touretzky, C. R., Johansson, T., Harjunkski, I., and Baldea, M. (2016). Optimal process operations in fast-changing electricity markets: Framework for scheduling with low-order dynamic models and an air separation application. *Industrial & Engineering Chemistry Research*, 55(16):4562–4584.
- Rothfuß, R. (1997). *Anwendung der flachheitsbasierten Analyse und Regelung nichtlinearer Mehrgrößen-systeme*. VDI-Verl., Düsseldorf.
- Rothfuß, R., Rudolph, J., and Zeitz, M. (1996). Flatness based control of a nonlinear chemical reactor model. *Automatica*, 32(10):1433–1439.
- Sass, S., Faulwasser, T., Hollermann, D. E., Kappatou, C. D., Sauer, D., Schütz, T., Shu, D. Y., Bardow, A., Gröll, L., Hagenmeyer, V., Müller, D., and Mitsos, A. (2020). Model compendium, data, and optimization benchmarks for sector-coupled energy systems. *Computers & Chemical Engineering*, 135:106760.
- Schulze, M. and Schenkendorf, R. (2020). Robust model selection: Flatness-based optimal experimental design for a biocatalytic reaction. *Processes*, 8(2).
- Schweidtmann, A. M., Weber, J. M., Wende, C., Netze, L., and Mitsos, A. (2021). Obey validity limits of data-driven models through topological data analysis and one-class classification. *Optimization and Engineering*.
- Schäfer, P., Daun, T. M., and Mitsos, A. (2020). Do investments in flexibility enhance sustainability? A simulative study considering the german electricity sector. *AIChE Journal*, 66(11):e17010.
- Simkoff, J. M. and Baldea, M. (2020). Stochastic scheduling and control using data-driven nonlinear dynamic models: Application to demand response operation of a chlor-alkali plant. *Industrial & Engineering Chemistry Research*.
- Unger, J., Kröner, A., and Marquardt, W. (1995). Structural analysis of differential-algebraic equation systems—theory and applications. *Computers & Chemical Engineering*, 19(8):867–882.
- Virtanen, P., Gommers, R., Oliphant, T. E., Haberland, M., Reddy, T., Cournapeau, D., Burovski, E., Peterson, P., Weckesser, W., Bright, J., van der Walt, S. J., Brett, M., Wilson, J., Millman, K. J., Mayorov, N., Nelson, A. R. J., Jones, E., Kern, R., Larson, E., Carey, C. J., Polat, İ., Feng, Y., Moore, E. W., VanderPlas, J., Laxalde, D., Perktold, J., Cimrman, R., Henriksen, I., Quintero, E. A., Harris, C. R., Archibald, A. M., Ribeiro, A. H., Pedregosa, F., van Mulbregt, P., and SciPy 1.0 Contributors (2020). SciPy 1.0: Fundamental Algorithms for Scientific Computing in Python. *Nature Methods*, 17:261–272.
- Voll, P., Klaffke, C., Hennen, M., and Bardow, A. (2013). Automated superstructure-based synthesis and optimization of distributed energy supply systems. *Energy*, 50:374–388.
- Zhang, Q. and Grossmann, I. E. (2016). Planning and scheduling for industrial demand side management: Advances and challenges. In Martín, M. M., editor, *Alternative Energy Sources and Technologies*, Engineering, pages 383–414. Springer, Switzerland.
- Zhang, Q., Grossmann, I. E., Sundaramoorthy, A., and Pinto, J. M. (2016). Data-driven construction of convex region surrogate models. *Optimization and Engineering*, 17(2):289–332.
- Zhou, D., Zhou, K., Zhu, L., Zhao, J., Xu, Z., Shao, Z., and Chen, X. (2017). Optimal scheduling of multiple sets of air separation units with frequent load-change operation. *Separation and Purification Technology*, 172:178–191.

Demand Response for Flat Nonlinear MIMO Processes using Dynamic Ramping Constraints - Supplementary Information

Florian Joseph Baader^{a,b,c,*}, Philipp Althaus^{a,c}, André Bardow^{a,b}, Manuel Dahmen^a

^a Forschungszentrum Jülich GmbH, Institute of Energy and Climate Research, Energy Systems Engineering (IEK-10), Jülich 52425, Germany

^b ETH Zürich, Energy & Process Systems Engineering, Zürich 8092, Switzerland

^c RWTH Aachen University Aachen 52062, Germany

1 Exemplary model for necessary flatness conditions

In this section, the two necessary conditions for flatness (compare to Section 3.2.1 in the main paper) are illustrated using an example (E) with three states and two inputs:

$$\dot{x}_1 = -x_1 - u_1 \quad (\text{Ea})$$

$$\dot{x}_2 = -x_2 + x_1 + u_2 \quad (\text{Eb})$$

$$\dot{x}_3 = -x_3 + 2x_1 - u_2 \quad (\text{Ec})$$

In the example (E), the output vector $\xi = (x_1, x_2)^T$ does not fulfil the necessary graphical condition for flat outputs because the state x_3 is not covered (Figure S1, center). However, the vector $\xi = (x_3, x_2)^T$ is a candidate for a flat output as all states are covered (Figure S1, right).

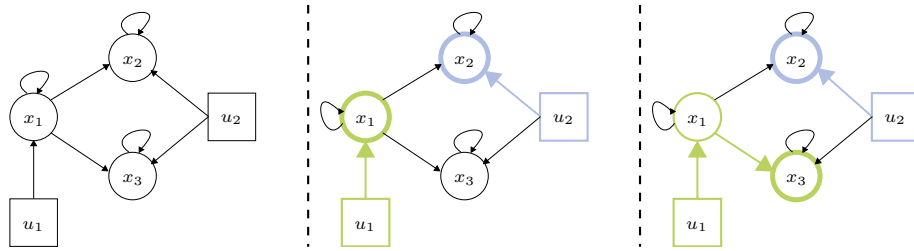


Fig. S1. Graph representation of example process (E) (left). While the candidate $\xi = (x_1, x_2)^T$ does not fulfil the necessary condition for a flat output vector (center), the candidate $\xi = (x_3, x_2)^T$ does (right).

To receive the equation system for the backtransformations, the flat output candidate $\xi = \phi(\mathbf{x}) = \begin{pmatrix} x_3 \\ x_2 \end{pmatrix}$ has to be differentiated two times to obtain a square backtransformation equation system:

$$\xi = \phi(\mathbf{x}) = \begin{pmatrix} x_3 \\ x_2 \end{pmatrix} \quad (\text{S1})$$

$$\dot{\xi} = \frac{\partial \phi(\mathbf{x})}{\partial \mathbf{x}} \dot{\mathbf{x}} = \frac{\partial}{\partial \mathbf{x}} \begin{pmatrix} x_3 \\ x_2 \end{pmatrix} \mathbf{f}(\mathbf{x}, \mathbf{u}) \quad (\text{S2})$$

$$\xi^{(2)} = \frac{\partial \dot{\xi}}{\partial \mathbf{x}} \dot{\mathbf{x}} + \frac{\partial \dot{\xi}}{\partial \mathbf{u}} \dot{\mathbf{u}} \quad (\text{S3})$$

Structurally, the backtransformation equation system (S1) - (S3) is solvable for the three states x_1, x_2, x_3 , the two inputs u_1, u_2 , and the input derivative \dot{u}_2 (Table S1). The input derivative \dot{u}_2 is part of the equation system as both second derivatives $\xi_1^{(2)}, \xi_2^{(2)}$ are functions of \dot{u}_2 .

2 Illustrative example for multiple feasible regions

As discussed in Section 3.4 of the main manuscript, multiple distinct feasible regions can occur for the dynamic ramping constraints. To illustrate this phenomenon, we consider an illustrative model (IM) with

*F. J. Baader, ETH Zürich, Energy & Process Systems Engineering, Zürich 8092, Switzerland
E-mail: fbaader@ethz.ch

Tab. S1. Analysis of structural solvability of the backtransformation equation system to calculate states \mathbf{x} , and inputs \mathbf{u} with flat output candidate $\boldsymbol{\xi} = (x_3, x_2)^T$ for example process (E). All states and inputs that appear in an equation are marked with a cross. A necessary condition for solvability is that it must be possible to circle exactly one cross in every row and exactly one cross in every line. In other words: Each equation should be solved for one variable.

	states			inputs and derivatives		
	x_1	x_2	x_3	u_1	u_2	\dot{u}_2
ξ_1			(x)			
ξ_2		(x)				
$\dot{\xi}_1$	(x)		x		x	
$\dot{\xi}_2$	x	x			(x)	
$\xi_1^{(2)}$	x		x	(x)	x	x
$\xi_2^{(2)}$	x	x		x	x	(x)

three states \mathbf{x} , two inputs \mathbf{u} , and a production rate ρ :

$$\dot{x}_1 = x_2 + \rho \quad (\text{IMa})$$

$$\dot{x}_2 = -x_2 + u_1 \quad (\text{IMb})$$

$$\dot{x}_3 = x_2^2 + u_2 \quad (\text{IMc})$$

As shown in the following, this process has a flat output $\boldsymbol{\xi} = \boldsymbol{\phi}(\mathbf{x}) = \begin{pmatrix} x_1 \\ x_3 \end{pmatrix}$. We assume an operating strategy $\boldsymbol{\xi} = \boldsymbol{\pi}(\rho) = \begin{pmatrix} a\rho \\ b\rho \end{pmatrix}$ with two constants a, b .

For x_1 , and x_3 , the back transformation is given by the function $\boldsymbol{\pi}$. For x_2 , Equation (IMa) is set equal to $\dot{\xi}_1 = \dot{x}_1 = a\dot{\rho}$ which gives

$$x_2 = \underbrace{a\dot{\rho}}_{\dot{x}_1} - \rho \quad (\text{S4})$$

Similarly, inserting $\dot{x}_2 = a\rho^{(2)} - \dot{\rho}$ into Equation (IMb) gives

$$u_1 = \underbrace{a\dot{\rho} - \rho}_{x_2} + \underbrace{a\rho^{(2)} - \dot{\rho}}_{\dot{x}_2} \quad (\text{S5})$$

Finally, inserting $\dot{\xi}_2 = \dot{x}_3 = b\dot{\rho}$ into Equation (IMc) gives

$$u_2 = \underbrace{b\dot{\rho}}_{\dot{x}_3} - \left(\underbrace{a\dot{\rho} - \rho}_{x_2} \right)^2 \quad (\text{S6})$$

As all states and inputs can be given as functions of production rate ρ and derivatives $\dot{\rho}, \rho^{(2)}$, the process is de facto flat for the given operating strategy.

Two feasible regions for the dynamic ramping constraints can result from the second input u_2 being a quadratic function of the first derivative of the production rate $\dot{\rho}$ (Equation (S6)) (Figure S2). One could either restrict the operating range to one of the two regions or would have to introduce a binary variable that indicates which region is active.

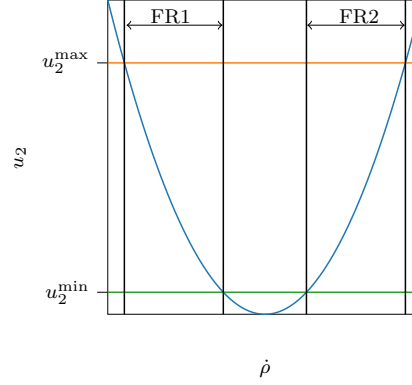


Fig. S2. Sketch for the input u_2 as function of the first derivative of the production rate $\dot{\rho}$ (compare to Equation (S6)). Potentially, there can be two feasible regions for $\dot{\rho}$, FR1 and FR2, respectively.

3 Supplementary information to case study

3.1 Model equations

In this section, we present the model equations of the case study (compare to Figure 4 in the main paper). All symbols other than states $\mathbf{x} = (c_{A1}, c_{B1}, T_1, c_{A2}, c_{B2}, T_2)^T$, control inputs $\mathbf{u} = (F_B, F_p, Q_1, Q_2)^T$, and production rate ρ are parameters marked in gray with values listed in Table S2. The index 0 indicates the feed quantities.

$$\dot{c}_{A1} = \frac{\rho + F_p}{V_1}(c_{A0} - c_{A1}) + \frac{F_B - F_p}{V_1}(c_{A2} - c_{A1}) - k_1 c_{A1} e^{-\frac{E_1}{RT_1}} \quad (\text{S7})$$

$$\begin{aligned} \dot{c}_{B1} = & \frac{\rho + F_p}{V_1}(c_{B0} - c_{B1}) + \frac{F_B - F_p}{V_1}(c_{B2} - c_{B1}) \\ & + k_1 c_{A1} e^{-\frac{E_1}{RT_1}} - k_2 c_{B1} e^{-\frac{E_2}{RT_1}} \end{aligned} \quad (\text{S8})$$

$$\begin{aligned} \dot{T}_1 = & \frac{\rho + F_p}{V_1}(T_0 - T_1) + \frac{F_B - F_p}{V_1}(T_2 - T_1) - \frac{\Delta H_1}{C_p} k_1 c_{A1} e^{-\frac{E_1}{RT_1}} \\ & - \frac{\Delta H_2}{C_p} k_2 c_{B1} e^{-\frac{E_2}{RT_1}} + \frac{Q_1}{\varrho_F C_p V_1} \end{aligned} \quad (\text{S9})$$

$$\dot{c}_{A2} = \frac{\rho + F_B}{V_2}(c_{A1} - c_{A2}) - \quad (\text{S10})$$

$$\begin{aligned} & \frac{\rho}{V_2} \left(\frac{\alpha_A c_{A2}}{\alpha_A c_{A2} + \alpha_B c_{B2} + \alpha_C (1 - c_{A2} - c_{B2})} - c_{A2} \right) \\ \dot{c}_{B2} = & \frac{\rho + F_B}{V_2}(c_{B1} - c_{B2}) \end{aligned} \quad (\text{S11})$$

$$\begin{aligned} & - \frac{\rho}{V_2} \left(\frac{\alpha_B c_{B2}}{\alpha_A c_{A2} + \alpha_B c_{B2} + \alpha_C (1 - c_{A2} - c_{B2})} - c_{B2} \right) \\ \dot{T}_2 = & \frac{\rho + F_B}{V_2}(T_1 - T_2) - \Delta H_V \frac{\rho}{\varrho_F C_p V_2} + \frac{Q_2}{\varrho_F C_p V_2} \end{aligned} \quad (\text{S12})$$

3.2 Operating strategy

As discussed in the main paper, the fourth flat output ξ_4 can be chosen freely. Here, we calculate the optimal steady-state operating points for ξ_4 and fix ξ_4 to be a function of the production rate $\xi_4 = \pi_4(\rho)$.

Tab. S2. Parameters of the reactor-separator process with recycle.

	symbol	value
volume CSTR	V_1	30 m^3
feed concentration A	c_{A0}	1
reaction constant reaction 1	k_1	$3.21 \times 10^6 \frac{1}{\text{h}}$
activation energy reaction 1	E_1	$5 \times 10^4 \frac{\text{kJ}}{\text{kmol}}$
gas constant	R	$8.314 \frac{\text{kJ}}{\text{kmolK}}$
feed concentration B	c_{B0}	0
reaction constant reaction 2	k_2	$3.21 \times 10^6 \frac{1}{\text{h}}$
activation energy reaction 2	E_2	$6 \times 10^4 \frac{\text{kJ}}{\text{kmol}}$
feed temperature	T_0	300 K
reaction enthalpy 1	ΔH_1	$-261 \frac{\text{kJ}}{\text{kg}}$
heat capacity	C_p	$4.2 \frac{\text{kJ}}{\text{kgK}}$
reaction enthalpy 2	ΔH_2	$-304 \frac{\text{kJ}}{\text{kg}}$
density	ρ_F	$1000 \frac{\text{kg}}{\text{m}^3}$
volume flash	V_2	30 m^3
relative volatility of A	α_A	0.5
relative volatility of B	α_B	0.25
relative volatility of C	α_C	1
enthalpy of vaporization	ΔH_V	$7.2 \times 10^4 \frac{\text{kJ}}{\text{kg}}$

Accordingly, we minimize the total heat input to the process $Q_1 + Q_2$ as the objective function to obtain the steady-state operating points. First, we determine the optimal steady-state operating points. To this end, a steady-state optimization problem (P_s) is formulated by sampling the production range $\rho^{\min} \leq \rho \leq \rho^{\max}$ with 21 equally distributed points ρ_j . The optimization problem (P_s) reads:

$$\begin{aligned}
& \min_{\mathbf{x}_j, \mathbf{u}_j} \sum_{j=1}^{21} Q_{1,j} + Q_{2,j} & (P_s a) \\
& \text{s.t. } \mathbf{0} = \mathbf{f}(\mathbf{x}_j, \mathbf{u}_j, \rho_j) & \forall j & (P_s b) \\
& \phi_{k,j}(\mathbf{x}) = \xi_k^{\text{nom}} & \forall k = 1, 2, 3 \forall j & (P_s c) \\
& \mathbf{u}^{\min} \leq \mathbf{u}_j \leq \mathbf{u}^{\max} & \forall j & (P_s d) \\
& \mathbf{x}^{\min} \leq \mathbf{x}_j \leq \mathbf{x}^{\max} & \forall j & (P_s e)
\end{aligned}$$

For every point j , the process needs to be in steady state (Equation ($P_s b$)), the first three flat output components $\xi_k = \phi_k(\mathbf{x})$ need to be at their nominal values (Equation ($P_s c$)), and inputs and states needs to be within bounds (Constraints ($P_s d$), ($P_s e$)). All bounds are given in Table S4. We implement the optimization problem P_s using pyomo (Hart et al., 2017) and solve it using BARON version 20.10.16 (Khajavirad and Sahinidis, 2018) in heuristic mode.

Next, a function $\pi_4(\rho)$ needs to be chosen that does not increase the objective function ($P_s a$) too much. In other words, the steady-state operation points reached with the additional constraint

$$\xi_{4,j} = \pi_4(\rho_j) \quad \forall j \quad (P_s f)$$

should give an objective function close to the objective function reached without the additional constraint ($P_s f$). As a first candidate, we investigate the simplest possible operating strategy, that is to hold ξ_4 constant, i.e., $\pi_4(\rho) = \xi_4^{\text{nom}}$. This optimization leads to a feasible solution. Accordingly, it is feasible to always hold the fourth flat output component at a constant value. However, the objective function worsens by 2.9 % compared to the first optimization without constraint ($P_s f$) because it is not possible to choose a single constant value ξ_4^{nom} that is optimal for all operating points. As a second candidate,

Tab. S3. Analysis of structural solvability with flat output candidate $\xi = (c_{A2}, c_{B2}, T_2, c_{A2})^T$ for the reactor-separator cycle (compare to Table S1).

	states						control inputs and derivatives						
	c_{A1}	c_{B1}	T_1	c_{A2}	c_{B2}	T_2	F_B	F_p	Q_1	Q_2	\dot{F}_B	\dot{F}_p	$F_B^{(2)}$
ξ_1				(X)									
ξ_2					(X)								
ξ_3						(X)							
ξ_4	(X)												
ξ_1	x			x	x		(X)						
ξ_2		(X)		x	x		x						
ξ_3			x			x	x			(X)			
ξ_4	x		(X)	x			x	x					
$\xi_1^{(2)}$	x	x	x	x	x		x	x			(X)		
$\xi_2^{(2)}$	x	x	x	x	x		x	(X)			x		
$\xi_4^{(2)}$	x	x	x	x	x	x	x	x	(X)		x	x	
$\xi_1^{(3)}$	x	x	x	x	x	x	x	x	x		x	x	(X)
$\xi_2^{(3)}$	x	x	x	x	x	x	x	x	x		x	(X)	x

Tab. S4. State and input bounds

variable	lower bound	upper bound
c_{A1}	0	1
c_{B1}	0	1
T_1	410 K	460K
F_B	$0 \frac{m^3}{h_s}$	$20 \frac{m^3}{h_s}$
F_p	$0 \frac{m^3}{h_s}$	$8 \frac{m^3}{h_s}$
Q_1	$0 \frac{kJ}{h_s}$	$10 \times 10^6 \frac{kJ}{h_s}$
Q_2	$0 \frac{kJ}{h_s}$	$4 \times 10^6 \frac{kJ}{h_s}$
ρ	$4.2 \frac{m^3}{h}$	$6.3 \frac{m^3}{h}$

we therefore investigate the linear strategy

$$\xi_4 = \pi_4(\rho) = a_0^{\xi_4} + a_1^{\xi_4} \rho, \quad (S13)$$

with optimization degrees of freedom $a_0^{\xi_4}$, $a_1^{\xi_4}$. The optimization finds values $a_0^{\xi_4}$, $a_1^{\xi_4}$ such that the objective value worsens only 0.05 % compared to the first optimization without the coupling constraint ($P_s f$). As this linear strategy is very close to the objective value found without constraint ($P_s f$), we do not consider other functions, e.g., higher-order polynomials, and continue with the linear operating strategy (S13).

3.3 Derivation of flat process reformulation

In this section, the nonlinear coordinate transformation is derived based on the nonlinear system of equations and the operating strategy. The aim is to express the states $\mathbf{x} = (c_{A1}, c_{B1}, T_1, c_{A2}, c_{B2}, T_2)^T$ and control inputs $\mathbf{u} = (F_B, F_p, Q_1, Q_2)^T$ as functions of production rate ρ , and its first two derivatives $\dot{\rho}$, and $\ddot{\rho}$.

For the reformulation, first, the strategy for the 4 flat output components $\xi = (c_{A2}, c_{B2}, T_2, c_{A1})^T$

discussed in Section 4.2 of the main manuscript is inserted:

$$c_{A2} = c_{A2}^{\text{nom}} \quad (\text{S14})$$

$$c_{B2} = c_{B2}^{\text{nom}} \quad (\text{S15})$$

$$T_2 = T_2^{\text{nom}} \quad (\text{S16})$$

$$c_{A1}(\rho) = a_0^{\xi_4} + a_1^{\xi_4} \rho \quad (\text{Equation (S13)}) \quad (\text{S17})$$

While the first three outputs are chosen independent of the production rate, the fourth output c_{A1} is a function of the production rate ρ .

Next, we consider the equation for the derivative of the first flat output, i.e., $\dot{\xi}_1 = \dot{c}_{A2}$. As c_{A2} is held constant, the derivative \dot{c}_{A2} is zero and we solve Equation (S10) for the bottom flow F_B that is a function of the production rate ρ , i.e.,

$$F_B(\rho) = \rho \left(\frac{c_{Av}^{\text{nom}} - c_{A2}^{\text{nom}}}{c_{A1}(\rho) - c_{A2}^{\text{nom}}} - 1 \right), \quad (\text{S18})$$

$$\text{with } c_{Av}^{\text{nom}} = \frac{\alpha_A c_{A2}^{\text{nom}}}{\alpha_A c_{A2}^{\text{nom}} + \alpha_B c_{B2}^{\text{nom}} + \alpha_C (1 - c_{A2}^{\text{nom}} - c_{B2}^{\text{nom}})},$$

and $c_{A1}(\rho)$ as defined in Equation (S17).

The second output is maintained constant, too. Accordingly, we receive the condition $\dot{\xi}_2 = \dot{c}_{B2} = 0$. After inserting $F_B(\rho)$ from Equation (S18) into Equation (S11), we get the equation:

$$0 = \frac{\rho ((c_{A1}(\rho) - c_{A2}^{\text{nom}})(c_{B2}^{\text{nom}} - c_{Bv}^{\text{nom}}) + (-c_{A2}^{\text{nom}} + c_{Av}^{\text{nom}})(c_{B1} - c_{B2}^{\text{nom}}))}{V_2 (c_{A1}(\rho) - c_{A2}^{\text{nom}})} \quad (\text{S19})$$

$$\text{with } c_{Bv}^{\text{nom}} = \frac{\alpha_B c_{B2}^{\text{nom}}}{\alpha_A c_{A2}^{\text{nom}} + \alpha_B c_{B2}^{\text{nom}} + \alpha_C (1 - c_{A2}^{\text{nom}} - c_{B2}^{\text{nom}})}$$

As ρ is always nonzero, we get c_{B1} as:

$$c_{B1}(\rho) = \frac{c_{A1}(\rho)c_{B2}^{\text{nom}} - c_{A1}(\rho)c_{Bv}^{\text{nom}} + c_{A2}^{\text{nom}}c_{Bv}^{\text{nom}} - c_{Av}^{\text{nom}}c_{B2}^{\text{nom}}}{c_{A2}^{\text{nom}} - c_{Av}^{\text{nom}}} \quad (\text{S20})$$

From the third output component, we get the condition $\dot{\xi}_3 = \dot{T}_2 = 0$ and thus solve Equation (S12) for Q_2 :

$$Q_2(\rho, T_1) = -\varrho_F C_p (\rho + F_B(\rho))(T_1 - T_2^{\text{nom}}) + \Delta H_V \rho. \quad (\text{S21})$$

The input Q_2 still depends on the temperature T_1 for which no expression has been derived up to this point.

From the fourth flat output component, we get $\dot{\xi}_4 = \dot{c}_{A1} = a_1^{\xi_4} \dot{\rho}$ (compare to Equation (S17)) and thus Equation (S7) changes to:

$$\begin{aligned} a_1^{\xi_4} \dot{\rho} = & -c_{A1}(\rho) k_1 e^{-\frac{E_1}{RT_1}} + \frac{(F_B(\rho) - F_p)(-c_{A1}(\rho) + c_{A2}^{\text{nom}})}{V_1} \\ & + \frac{(F_p + \rho)(c_{A0} - c_{A1}(\rho))}{V_1} \end{aligned} \quad (\text{S22})$$

Equation (S22) is solved numerically for T_1 . However, first, an expression for the input F_p is needed. This expression is derived from the condition that according to our operating strategy the second derivative of the second output is zero, i.e., $\xi_2^{(2)} = c_{B2}^{(2)} = 0$. From this condition, we receive

$$F_p(\rho, T_1) = \Psi_{F_p}(\rho, T_1), \quad (\text{S23})$$

with a nonlinear function $\Psi_{F_p}(\rho, T_1)$, which is not stated here to preserve readability. After inserting Equation (S23) into Equation (S22), Equation (S22) implicitly defines T_1 as a function of ρ and $\dot{\rho}$, $T_1(\rho, \dot{\rho})$.

As discussed in the main paper, we cannot solve for T_1 analytically, but the solution received numerically is unique. With $T_1(\rho, \dot{\rho})$, we can calculate Q_2 as $Q_2(\rho, \dot{\rho})$ (compare to Equation (S21)) and F_p as $F_p(\rho, \dot{\rho})$ (compare to Equation (S23)).

The only variable that is missing is the reactor heating Q_1 . To get an expression for Q_1 , Equation (S22) is differentiated with respect to time. Before doing so, we replace F_p with $\Psi_{F_p}(\rho, T_1)$ (compare to Equation (S23)) and insert the functions for F_B and $c_{A,1}$, which depend on ρ . After bringing everything to the left hand side, Equation (S22) changes to

$$0 = \Psi(\rho, \dot{\rho}, T_1). \quad (\text{S24})$$

Building the total differential with respect to time gives

$$\begin{aligned} 0 &= \frac{\partial \Psi(\rho, \dot{\rho}, T_1)}{\partial \rho} \dot{\rho} + \frac{\partial \Psi(\rho, \dot{\rho}, T_1)}{\partial \dot{\rho}} \nu + \frac{\partial \Psi(\rho, \dot{\rho}, T_1)}{\partial T_1} \left[\frac{\rho + F_p}{V_1} (T_0 - T_1) + \right. \\ &\quad \left. \frac{F_B - F_p}{V_1} (T_2 - T_1) - \frac{\Delta H_1}{C_p} k_1 c_{A1} e^{-\frac{E_1}{RT_1}} - \frac{\Delta H_2}{C_p} k_2 c_{B1} e^{-\frac{E_2}{RT_1}} + \frac{Q_1}{\rho_F C_p V_1} \right] \\ &= \Psi_0(\rho, \dot{\rho}, T_1) + \Psi_\nu(\rho, \dot{\rho}, T_1) \nu + \Psi_{Q_1}(\rho, \dot{\rho}, T_1) Q_1 \\ &\quad \text{with } \Psi_\nu(\rho, \dot{\rho}, T_1) = \frac{\partial \Psi(\rho, \dot{\rho}, T_1)}{\partial \dot{\rho}}, \Psi_{Q_1}(\rho, \dot{\rho}, T_1) = \frac{\partial \Psi(\rho, \dot{\rho}, T_1)}{\partial T_1} \frac{1}{\rho_F C_p V_1}, \\ &\quad \text{and } \Psi_0(\rho, \dot{\rho}, T_1) \text{ as the remaining part.} \end{aligned} \quad (\text{S25})$$

As Q_1 enters linearly, we can easily solve Equation (S25) for Q_1 . Moreover, the ramping degree of freedom ν enters linearly as well, which allows to solve Equation (S25) for ν and calculate the bounds of ν from the bounds of Q_1 (compare to Figure S3).

At this point, all states and inputs can be calculated as functions of the production rate ρ and its first two derivatives $\dot{\rho}$, and ν .

Note that we do not derive expressions for the input derivatives \dot{F}_B , $F_B^{(2)}$, and \dot{F}_p that are shown in Table S3. Instead, we replace F_B with $F_B(\rho)$ (Equation (S18)), and F_p with $F_p(\rho, T_1)$ (Equation (S23)) in the equations where they appear and subsequently differentiate the complete equations with respect to time.

3.4 Calculating the limits for $\dot{\rho}$

As discussed in the previous section, the limits for ν can be calculated in a straightforward way from Equation (S25). In this section, we calculate the limits for $\dot{\rho}$ resulting from the bounds of T_1 , Q_2 , F_p (Figure 6 in the main paper). First, the bounds are calculated as a function of T_1 by dividing Equation (S22) by $a_1^{\xi_4}$, giving $\dot{\rho}$ as

$$\dot{\rho} = \theta_{T_1}(\rho, T_1), \quad (\text{S26})$$

with a nonlinear function θ_{T_1} . Note that while Equation (S22) cannot be solved for T_1 analytically, Equation (S22) can be solved analytically for $\dot{\rho}$. Accordingly, inserting the bounds of T_1 gives the limits of $\dot{\rho}$ shown in Figure 6 in the main paper.

In the case of Q_2 , which is calculated as $Q_2(\rho, T_1)$ from Equation (S21), Equation (S21) cannot be solved for $\dot{\rho}$ as no analytic expression was derived for T_1 that depends on ρ and $\dot{\rho}$. Instead, Equation (S21) is solved for T_1 as $T_1(Q_2, \rho)$, which is straightforward as T_1 enters Equation (S21) linearly. Inserting $T_1(Q_2, \rho)$ into Equation (S26) then gives

$$\dot{\rho} = \theta_{T_1}(\rho, T_1(Q_2, \rho)), \quad (\text{S27})$$

which allows to calculate the limits of $\dot{\rho}$ from the bounds of Q_2 as shown in Figure 6 in the main paper.

For the purge stream F_p , we follow the same strategy to first calculate T_1 and then $\dot{\rho}$. However, Equation (S23) cannot be solved for T_1 as function of F_p and ρ analytically due to the exponential functions (see discussion around Equation (11) in main paper). Consequently, Equation (S23) is solved numerically for T_1 as function of the bounds on F_p . This value of T_1 is then used to calculate the limits of $\dot{\rho}$ shown in Figure 6 in the main paper.

3.5 Ramping limits on ν

In this section, the derivation of the ramping limits on the ramping degree of freedom ν is given in detail. First, the space given by the limits ρ^{\min} , ρ^{\max} and $\dot{\rho}^{\min}(\rho)$, $\dot{\rho}^{\max}(\rho)$ is sampled using 51×51 points. For every point, the true limits $\nu_{\text{true}}^{\min}(\rho, \dot{\rho})$, $\nu_{\text{true}}^{\max}(\rho, \dot{\rho})$ are calculated from Q_1^{\min} , Q_1^{\max} (compare to Equation (S25)) (Figure S3). For a conservative approximation of these limits, we use piecewise affine

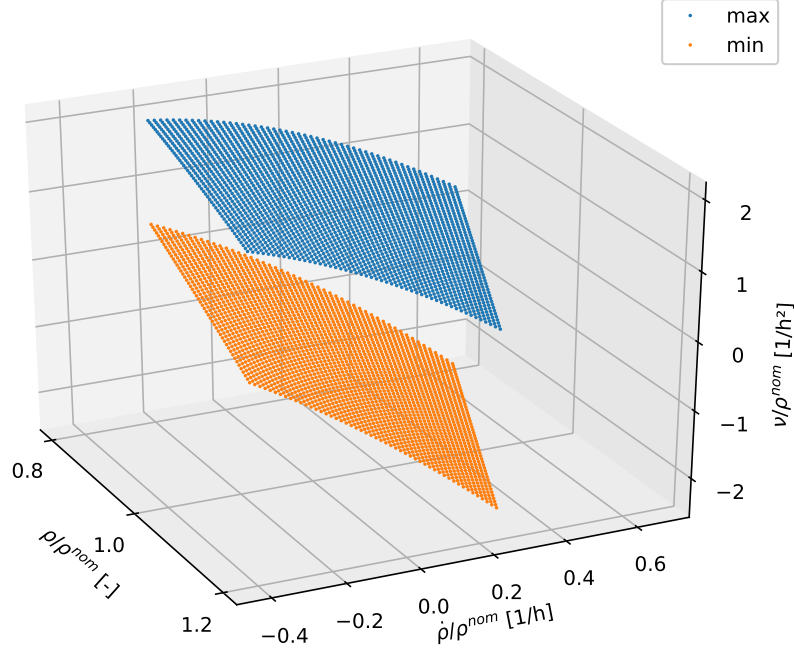


Fig. S3. True limits on the ramping degree of freedom ν dependent on production rate ρ and its first time derivative $\dot{\rho}$. All values are normalized with the nominal production rate ρ^{nom}

functions. We distinguish between production rates ρ above and below the nominal rate ρ^{nom} , and first derivatives $\dot{\rho}$ above and below zero. Thus, the piecewise affine functions have 4 segments and need 2 binary variables in the optimization: z_ρ indicating if ρ is above or below the nominal rate ρ^{nom} , and $z_{\dot{\rho}}$ indicating if $\dot{\rho}$ is above or below zero. In every segment s , the limits $\nu_{\text{PWA}}^{\min}(\rho, \dot{\rho})$, $\nu_{\text{PWA}}^{\max}(\rho, \dot{\rho})$ are given as

$$\nu_{\text{PWA},s}^{\min}(\rho, \dot{\rho}) = a_{0,s}^{\min} + a_{\rho,s}^{\min} \rho + a_{\dot{\rho},s}^{\min} \dot{\rho}, \quad (\text{S28})$$

$$\nu_{\text{PWA},s}^{\max}(\rho, \dot{\rho}) = a_{0,s}^{\max} + a_{\rho,s}^{\max} \rho + a_{\dot{\rho},s}^{\max} \dot{\rho}, \quad (\text{S29})$$

with parameters $a_{0,s}^{\min}$, $a_{\rho,s}^{\min}$, $a_{\dot{\rho},s}^{\min}$, $a_{0,s}^{\max}$, $a_{\rho,s}^{\max}$, $a_{\dot{\rho},s}^{\max}$. The parameters are calculated in an optimization, which minimizes the difference to the true bounds while ensuring conservativeness such that $\nu_{\text{true}}^{\min}(\rho, \dot{\rho}) \leq \nu_{\text{PWA},s}^{\min}(\rho, \dot{\rho}) < \nu_{\text{PWA},s}^{\max}(\rho, \dot{\rho}) \leq \nu_{\text{true}}^{\max}(\rho, \dot{\rho})$ holds for every point $(\rho, \dot{\rho})$.

To evaluate the quality of the bounds, we calculate the coverage $C(\rho, \dot{\rho})$:

$$C(\rho, \dot{\rho}) = \frac{\nu_{\text{PWA}}^{\max}(\rho, \dot{\rho}) - \nu_{\text{PWA}}^{\min}(\rho, \dot{\rho})}{\nu_{\text{true}}^{\max}(\rho, \dot{\rho}) - \nu_{\text{true}}^{\min}(\rho, \dot{\rho})}, \quad (\text{S30})$$

which is the distance between the chosen bounds in relation to the distance between the true bounds. The arithmetic mean of the coverage is 95 %. Accordingly, the chosen piecewise affine limits capture approximately 95 % of the feasible region. Therefore, we do not refine the approximation by introducing more segments.

3.6 Multi-energy system and optimization problem for demand response application

In this section, we describe the multi-energy system and the optimization problem in the second study, which considers a demand response application. Our aim for this case study is to construct an illustrative example that demonstrates the application and capabilities of our new method. The considered multi-energy system is based on the third day of the benchmark problem given by [Sass et al. \(2020\)](#). Note that the data are publicly available at [?](#). The given heat and electricity demands are multiplied by 3 as we increase the number of units from 2 to 6.

Instead of one combined heat and power plant (CHP) and one boiler (B) as in [Sass et al. \(2020\)](#), we use 4 CHPs and 2 boilers. All 4 CHPs have a nominal thermal output power of 450 kW, and the 2 boilers have 530 kW. The nominal efficiencies are given in Table S5.

Tab. S5. Nominal efficiencies of energy-system components.

unit	thermal efficiency	electric efficiency
B1	79.2%	-
B1	80.8%	-
CHP1	48.3%	37.7%
CHP2	49.3%	38.4%
CHP3	50.3%	39.2%
CHP4	51.3%	39.9%

The minimum part-load fraction is 50% for the CHPs and 20% for the boilers ([Sass et al., 2020](#)). Following [Voll \(2014\)](#), the part-load efficiency curves are discretized with one affine element to achieve an accurate discretization.

The electricity price used is the German day-ahead price from April 2nd, 2021 ([SMARD Marktdaten, 2021](#)). This price curve is chosen because it features times with low prices that make the operation of the boiler favorable and times of high prices which make the operation of the CHPs favorable.

For the optimization problem, which schedules the flexible operation of the reactor-separator process, a process energy demand model is needed (Pc). As the dynamic ramping constraint is second order, the heat demand of the process is modeled as a function of ρ , $\dot{\rho}$, and ν , i.e.,

$$Q_{\text{dem,heat}}^{\text{process}}(\rho, \dot{\rho}, \nu). \quad (\text{S31})$$

To fit the heat demand model, we sample the operating region given by the limits ρ^{\min} , ρ^{\max} , $\dot{\rho}^{\min}(\rho)$, $\dot{\rho}^{\max}(\rho)$, and $\nu^{\min}(\rho, \dot{\rho})$, $\nu^{\max}(\rho, \dot{\rho})$ using $11 \times 11 \times 11$ points. First, a purely linear function is used for the heat demand and the parameters are fitted using linear regression. Because the average absolute approximation error is 10% of the nominal heat demand, we try a piecewise-affine (PWA) model to increase the accuracy. For this new PWA model, the operating region is split into segments in which affine functions are used. Here, the operating region is split into four segments by making two distinctions: If $\dot{\rho}$ is greater or smaller than zero and if ν is greater or smaller than zero. To implement the PWA model in the optimization, two binary variables are needed: $z_{\dot{\rho}}$ indicates whether $\dot{\rho}$ is positive and z_{ν} indicates whether ν is positive. No distinction is made for ρ as we find that the heat demand is roughly linear with ρ . The PWA model reduces the mean approximation error to 5% of the nominal heat demand.

The optimization problem is discretized using orthogonal collocation with 2 elements per hour and 3 collocation points per element. The binary variables are discretized with one-hour timestep to match the hourly changing prices and demands. There are 9 binary variables per timestep: 4 on/off binaries for the CHPs, 2 on/off binaries for the boilers, 2 binaries z_{ρ} , $z_{\dot{\rho}}$ for the piecewise affine approximation of the ramping limits $\nu_{\text{PWA}}^{\min}(\rho, \dot{\rho})$, $\nu_{\text{PWA}}^{\max}(\rho, \dot{\rho})$, and 1 additional binary z_{ν} for the PWA heat demand model. Consequently, the optimization problem has $9 \times 24 = 216$ binary variables for the 24 h time horizon. The ramping degree of freedom ν is discretized to be piecewise linear for every hour.

Bibliography

- Hart, W. E., Laird, C. D., Watson, J.-P., Woodruff, D. L., Hackebeil, G. A., Nicholson, B. L., and Sirola, J. D. (2017). *Pyomo—Optimization modeling in Python*, volume 67. Springer Science & Business Media, second edition.
- Khajavirad, A. and Sahinidis, N. V. (2018). A hybrid LP/NLP paradigm for global optimization relaxations. *Mathematical Programming Computation*, 10(3):383–421.
- Sass, S., Faulwasser, T., Hollermann, D. E., Kappatou, C. D., Sauer, D., Schütz, T., Shu, D. Y., Bardow, A., Gröll, L., Hagenmeyer, V., Müller, D., and Mitsos, A. (2020). Model compendium, data, and optimization benchmarks for sector-coupled energy systems. *Computers & Chemical Engineering*, 135:106760.
- SMARD Marktdaten (2021). <https://www.smard.de/home/marktdaten> (accessed 01 April 2021).
- Voll, P. (2014). *Automated optimization-based synthesis of distributed energy supply systems*. PhD thesis, RWTH Aachen University.